A computational study of accelerating, steady and fading negative streamers in ambient air

Baohong Guo[1] **, Xiaoran Li**[1,2] **, Ute Ebert**[1,3] **and Jannis Teunissen**[1,*]

[1] Centrum Wiskunde & Informatica (CWI), Amsterdam, The Netherlands
[2] State Key Laboratory of Electrical Insulation and Power Equipment, School of Electrical Engineering, Xi'an Jiaotong University, Xi'an 710049, People's Republic of China
[3] Department of Applied Physics, Eindhoven University of Technology, Eindhoven, The Netherlands

E-mail: jannis.teunissen@cwi.nl

Abstract

We study negative streamers in ambient air using a 2D axisymmetric fluid model. Depending on the background electric field, we observe accelerating, steady and fading negative streamers. Fading occurs in low background fields, when negative streamers lose their field enhancement and when their velocities become comparable to their maximal electron drift velocities. Our focus is on the steady propagation mode, during which streamer properties like radius and velocity hardly change. However, this mode is unstable, in the sense that a small change in conditions leads to acceleration or deceleration. We observe steady negative streamers in background fields ranging from 9.19 kV cm^{-1} to 15.75 kV cm^{-1}, indicating that there is no unique steady propagation field (or stability field). Another finding is that steady negative streamers are able to keep propagating over tens of centimeters, with only a finite conductive length behind their heads, similar to steady positive streamers. Approximately linear relationships are observed between the optical diameter and properties like the streamer velocity and the streamer head potential. From these linear relations, we obtain rough lower bounds of about 0.27 mm to 0.35 mm for the minimal optical diameter of steady negative streamers. The lowest background field in which a steady negative streamer could be obtained is 9.19 kV cm^{-1}. In contrast, steady positive streamers have recently been obtained in a background field as low as 4.05 kV cm^{-1}. We find that the properties of steady negative and positive streamers differ significantly. For example, for steady negative streamers the ratio between streamer velocity and maximal electron drift velocity ranges from about 2 to 4.5, whereas for steady positive streamers this ratio ranges from about 0.05 to 0.26.

Keywords: negative streamer, stability field, steady streamer propagation, streamer stagnation, negative streamer fading

(Some figures may appear in colour only in the online journal)

1. Introduction

Streamer discharges are fast-moving ionization fronts with self-organized field enhancement at their tips [1]. This field enhancement allows them to propagate into regions where the background electric field is below breakdown [2]. Streamers are the precursors of sparks and lightning leaders [3, 4], and they exist in nature as so-called sprites [5, 6]. Streamers are widely observed in cold atmospheric plasma applications [7–9], as well as in high-voltage technology [10–12].

Streamers can have positive or negative polarity. Positive streamers in air have been studied and modelled more

---

* Author to whom any correspondence should be addressed.

frequently than negative ones because they initiate more easily [13, 14]. However, negative streamers also widely exist in nature and industry [15–22]. In experimental [13, 23–25] and computational [14, 26–30] comparisons between positive and negative streamers in the same background field, positive streamers in atmospheric-pressure air were typically faster and thicker than negative ones, with higher field enhancement at their heads and higher plasma densities in their channels. In higher background fields, these differences were smaller.

In this paper, we study the dynamics of negative streamer propagation in air with simulations. We focus on three main topics. First, we study negative streamer fading dynamics in weak background fields. Second, we look into steady streamer propagation, i.e., propagation with a constant velocity during which streamer properties hardly change. We study in particular how the properties of steady negative streamers vary with the background field. Third, we consider the relationships between steady negative streamer properties like diameter, velocity and maximal electric field, and we compare these properties to those of steady positive streamers.

There is a difference between negative streamer fading and positive streamer stagnation. A fading negative streamer loses its field enhancement, but electrons near the streamer head continue their drift motion. In contrast, a stagnating positive streamer will eventually come to an approximate halt due to the relative immobility of positive ions [31, 32], and its field enhancement tends to increase before stagnation.

There are relatively few experimental studies in which the propagation of negative streamers in air was captured. Most relevant for the present paper is the work of Briels *et al* [13], in which positive and negative streamers were studied at various voltages in a needle-to-plane gap of 4 cm. Negative streamers could form at voltages above 30 kV, and they could cross the gap at voltages above 56 kV. Negative streamers in air were also captured in [18], on microsecond time scales in a meter-sized gap, and in [33], in a wire-plate geometry.

Several authors have numerically studied the propagation of negative streamers. In [26], negative streamer deceleration was simulated in atmospheric air in weak uniform electric fields. In the numerical study of [28], a negative discharge in air at standard temperature and pressure was found to extinguish after less than 2 mm propagation in a low background field. However, the authors noted that a negative discharge of only 2 mm cannot be considered a fully developed streamer.

Recently, Starikovskiy *et al* [34] simulated decelerating streamers in 5 cm and 14 cm gaps for both voltage polarities. Regardless of the gap geometry, the authors found that a negative streamer in air decelerated with a decrease in the maximal electric field and an increase in the radius, and it eventually transformed to a discharge mode dominated by electron drift. Furthermore, they showed that the deceleration dynamics of negative and positive streamers were completely different.

From a numerical modelling point of view, negative streamer fading is easier to simulate than positive streamer stagnation. As pointed out in [34–36], the electric field can diverge when positive streamer stagnation is simulated using a fluid model with the local field approximation. Such problems can be avoided by using an extended fluid model [31] or by modifying the impact ionization source term [32].

To understand streamer propagation, the phenomenological concept of a 'stability field' has frequently been used [1, 3, 37, 38]. The stability field was defined as the background electric field required for steady streamer propagation [26, 32, 36, 39]. This field is here referred to as 'the steady propagation field'. More commonly, the stability field has been defined as the minimal electric field required for a streamer to cross a gap [3, 37, 40, 41]. As pointed out in [32, 39–44], both the steady propagation field and the stability field are not unique. They depend not only on factors such as the gas, humidity, and applied voltage polarity, but also on streamer properties like the velocity and radius. We will discuss the steady propagation field and the stability field in more detail in section 3.2.

Several observations have been made about the velocity–diameter relation of negative streamers in air. Experimentally, an empirical fit $v = 0.5d^2 \, \mathrm{mm}^{-1} \, \mathrm{s}^{-1}$ for both positive and negative streamers in ambient air at 1 bar was obtained in [13]. In contrast, a linear relationship between velocity and diameter was predicted in the analytical and numerical study of [29], if the maximal electric field at the streamer head was assumed constant, and if the relative increase of electron density at the streamer tip was fixed. However, deviations from linearity are to be expected, since the maximal electric field depends on factors such as the streamer radius and the applied voltage, and since the relative electron density increase can also vary.

The present study was performed in parallel with the one on steady positive streamers described in [32]. In both papers steady streamers with different properties were obtained, but using different methods. In [32], the applied voltage was changed in time to obtain certain constant streamer velocities. Here we instead use a DC applied voltage (constant in time). A voltage corresponding to steady propagation is found by performing simulations with different applied voltages. For given electrode and initial conditions we only find one such voltage, so we vary the electrode geometry to obtain different steady negative streamers.

The paper is organized as follows. In section 2, we describe the 2D axisymmetric fluid model, along with the chemical reactions and simulation conditions. The simulation results are presented in section 3. Accelerating, steady and fading negative streamers are investigated in different background fields. Then we discuss stability fields and steady propagation fields. We also study the steady propagation of negative streamers in different background fields. In section 4, we address several important questions about negative streamers, and compare their properties with those of positive streamers. Finally, we summarize our findings in section 5, and provide some ideas for future studies.

2. Simulation model

We use a 2D axisymmetric drift-diffusion-reaction type fluid model with the local field approximation to simulate single

Table 1. List of reactions included in the model, with reaction rate coefficients and references. The symbol M denotes a neutral molecule (either N_2 or O_2). E/N is the reduced electric field.

No.	Reaction	Reaction rate coefficient	Reference
Electron impact ionization			
R1	$e + N_2 \rightarrow e + e + N_2^+$ (15.60 eV)	$k_1(E/N)$	[50]
R2	$e + N_2 \rightarrow e + e + N_2^+$ (18.80 eV)	$k_2(E/N)$	[50]
R3	$e + O_2 \rightarrow e + e + O_2^+$ (12.06 eV)	$k_3(E/N)$	[50]
Electron attachment			
R4	$e + O_2 + O_2 \rightarrow O_2^- + O_2$	$k_4(E/N)$	[50]
R5	$e + O_2 \rightarrow O^- + O$	$k_5(E/N)$	[50]
Electron detachment			
R6	$O_2^- + M \rightarrow e + O_2 + M$	$k_6 = 1.24 \times 10^{-17} \exp(-(\frac{179}{8.8+E/N})^2)$ m^3 s^{-1}	[51]
R7	$O^- + N_2 \rightarrow e + N_2O$	$k_7 = 1.16 \times 10^{-18} \exp(-(\frac{48.9}{11+E/N})^2)$ m^3 s^{-1}	[51]
Negative ion conversion			
R8	$O^- + O_2 \rightarrow O_2^- + O$	$k_8 = 6.96 \times 10^{-17} \exp(-(\frac{198}{5.6+E/N})^2)$ m^3 s^{-1}	[51]
R9	$O^- + O_2 + M \rightarrow O_3^- + M$	$k_9 = 1.10 \times 10^{-42} \exp(-(\frac{E/N}{65})^2)$ m^6 s^{-1}	[51]
Electron excitation			
R10	$e + N_2 \rightarrow e + N_2(C^3\Pi_u)$	$k_{10}(E/N)$	[50]
Quenching			
R11	$N_2(C^3\Pi_u) + N_2 \rightarrow N_2 + N_2$	$k_{11} = 1.3 \times 10^{-17}$ m^3 s^{-1}	[52]
R12	$N_2(C^3\Pi_u) + O_2 \rightarrow O_2 + N_2$	$k_{12} = 3.0 \times 10^{-16}$ m^3 s^{-1}	[52]
Radiation			
R13	$N_2(C^3\Pi_u) \rightarrow N_2(B^3\Pi_g) + h\nu$	$k_{13} = 1/(42$ ns$)$	[52]

negative streamers in artificial dry air, consisting of 80% N_2 and 20% O_2, at 300 K and 1 bar. We use `Afivo-streamer` [45], an open-source code for streamer fluid simulations. The code is based on the Afivo framework [46], which includes adaptive mesh refinement (AMR), shared-memory (OpenMP) parallelism and a geometric multigrid solver. This code was compared to five other fluid simulation codes in the comparison study of [47]. Furthermore, simulations using `Afivo-streamer` were recently compared against experiments in [48], and compared against particle-in-cell simulations both in 2D and 3D for positive streamers in air in [49], which found good quantitative agreement.

2.1. Model equations

The temporal evolution of the electron density n_e is given by

$$\partial_t n_e = \nabla \cdot (\mu_e \mathbf{E} n_e + D_e \nabla n_e) + S_i - S_{att} + S_{det} + S_{ph}, \quad (1)$$

where μ_e is the electron mobility, $\mathbf{E}$ the electric field, D_e the electron diffusion coefficient, and S_i, S_{att}, S_{det} and S_{ph} are the source terms for electron impact ionization, electron attachment, electron detachment and non-local photoionization, respectively. The densities of other species involved in the model evolve according to the reactions listed in table 1. Ions and neutrals are assumed to be immobile due to their much larger mass than that of electrons. We therefore do not include ion motion in the model, as is discussed in appendix B.

The electric field $\mathbf{E}$ is calculated in the electrostatic approximation as

$$\mathbf{E} = -\nabla \phi, \quad (2)$$

where the electrostatic potential ϕ is obtained by solving Poisson's equation

$$\nabla^2 \phi = -\frac{\rho}{\varepsilon_0}, \quad (3)$$

where ρ is the space charge density and ε_0 is the vacuum permittivity.

2.2. Chemical reactions and input data

We use a relatively small set of chemical reactions, which are listed in table 1. Note that positive ion conversion and electron–ion recombination are not included. Such reactions can play an important role in air, for example due to the formation of O_4^+ with which electrons can dissociatively recombine, but in appendix C we show that they have a relatively minor effect on the negative streamers studied here. From table 1, the source terms for electron impact ionization, attachment and detachment are computed as

$$S_i = k_1 n_e[N_2] + k_2 n_e[N_2] + k_3 n_e[O_2], \quad (4)$$

$$S_{att} = k_4 n_e[O_2]^2 + k_5 n_e[O_2], \quad (5)$$

$$S_{det} = k_6[M][O_2^-] + k_7[N_2][O^-], \quad (6)$$

Table 2. Description of the two axisymmetric computational domains used in the present paper. z_{head} is the streamer position at which the electric field has a maximum, see section 2.5.

	Domain A	Domain B
Domain size (r, z)	125 mm, 125 mm	300 mm, 300 mm
Rod electrode	One fixed geometry	Ten different geometries
Rod electrode length L_{rod}	9.9 mm	3.3 mm to 26.4 mm
Rod electrode radius R_{rod}	0.9 mm	$L_{rod}/11$
Simulations stop when	$z_{head} = 30$ mm or fading	$z_{head} = 100$ mm or fading
Simulation results	sections 3.1–3.3	section 3.4

where k_i $(i = 1, 2, \ldots, 7)$ are the reaction rate coefficients, $[N_2]$, $[O_2]$, $[O^-]$ and $[O_2^-]$ are the species densities, and $[M] = [N_2] + [O_2]$. We assume that the number density of $[M]$ does not change in the model. Note that the three-body attachment reaction, $e + O_2 + N_2 \rightarrow O_2^- + N_2$, is not included in the model because its reaction rate coefficient is about two to three orders of magnitude smaller than k_4 [53].

Non-local photoionization in air occurs ahead of a streamer discharge when an UV photon ionizes an oxygen molecule at some isotropically distributed distance. The UV photon is emitted from an excited nitrogen molecule with a wavelength in the range 98–102.5 nm. Photoionization is typically considered as an important source of free electrons for both positive and negative streamers in air [14, 23, 26–29, 54]. Here we use Zheleznyak's model to describe photoionization [55]. Then the photoionization source term S_{ph} in equation (1) is given by

$$S_{ph}(\boldsymbol{r}) = \int \frac{I(\boldsymbol{r}')f(|\boldsymbol{r} - \boldsymbol{r}'|)}{4\pi|\boldsymbol{r} - \boldsymbol{r}'|^2} \, \mathrm{d}^3 r', \tag{7}$$

where $\boldsymbol{r}$ is a given observation point, $\boldsymbol{r}'$ the source point emitting UV photons, $I(\boldsymbol{r}')$ the source of ionizing photons, $f(|\boldsymbol{r} - \boldsymbol{r}'|)$ the photon absorption function, and $4\pi|\boldsymbol{r} - \boldsymbol{r}'|^2$ is a geometric factor. In Zheleznyak's model, $I(\boldsymbol{r}')$ is proportional to the electron impact ionization source term S_i given by equation (4) as

$$I(\boldsymbol{r}') = \frac{p_q}{p + p_q}\xi S_i, \tag{8}$$

where $p_q = 40$ mbar is the quenching pressure, p the gas pressure, and ξ is a proportionality factor, which is here set to $\xi = 0.075$ for simplicity as in [36, 48, 49, 56, 57], although it is in principle field-dependent [55]. We solve equation (7) using the so-called Helmholtz approximation [54, 58], for which the absorption function is computed from Bourdon's three-term expansion [58]. See the appendix of [47] for more information.

With the local field approximation, the electron velocity distribution is assumed to be relaxed to the local electric field. Therefore the transport coefficients μ_e and D_e, and the reaction rate coefficients $(k_1–k_{10})$ are functions of the reduced electric field E/N, where E is the electric field and N is the gas number density. These coefficients were computed with BOLSIG+, a two-term electron Boltzmann equation solver [59], using the temporal growth model. Electron-neutral scattering cross sections for N_2 and O_2 were obtained from the Phelps database [50, 60].
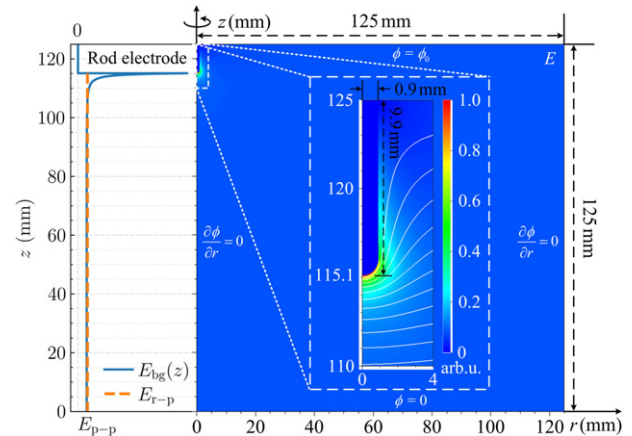

Figure 1. Schematic view of computational domain A. Right: the rod electrode geometry, boundary conditions for the electric potential ϕ and initial electric field E without a streamer. Left: the axial background electric field $E_{bg}(z)$ and the average electric field E_{r-p} between the rod electrode tip and the grounded electrode. E_{p-p} is the average electric field between the upper and lower plate electrodes.

2.3. Computational domains and initial conditions

We use two axisymmetric computational domains in the simulations, as described in table 2. Domain A measures 125 mm in the r and z directions, whereas domain B measures 300 mm in both directions. Both domains have a plate–plate geometry with a rod-shaped electrode of length L_{rod} placed at the centre of the upper plate, see figure 1. For domain A we use $L_{rod} = 9.9$ mm and for domain B we use ten different electrode lengths ranging from 3.3 mm to 26.4 mm. All electrodes have a semi-spherical tip and a radius R_{rod} given by $L_{rod}/11$, which means that longer electrodes are also wider. Also note that for longer electrodes, the distance between the electrode tip and the grounded electrode is shorter, but the electrode length is always significantly smaller than the domain length, see figure 1.

We apply the same initial and boundary conditions for both domains. A fixed electric potential ϕ_0 is applied on the upper domain boundary and the rod electrode. The lower domain boundary is grounded. A homogeneous Neumann boundary condition for the electric potential is applied on the outer axial boundary.

For the electron density, homogeneous Neumann boundary conditions are applied on all domain boundaries, including the

rod electrode. Secondary electron emission due to ions and photons is not included. It would be more realistic to only allow an outflow of electrons from the rod electrode due to secondary emission [30, 61]. However, this would give rise to very high electric fields around the rod electrode and steep density gradients, which are numerically challenging to simulate. The artificial boundary conditions used here affect discharge inception, and therefore also the initial streamer properties. However, we here focus on steady discharge evolution far from electrodes. For most of the cases we study the back part of the discharge has a low conductivity (see e.g. figure 7), so the artificial boundary conditions should not have a major effect on this steady propagation.

The axial background electric field $E_{bg}(z)$ in figure 1 is almost uniform, except for a small region near the rod electrode. Far away from the rod electrode, $E_{bg}(z)$ is almost equal to the average electric field E_{p-p} between the upper and lower plate electrodes. In addition, there is the average electric field E_{r-p} between the rod electrode tip and the grounded electrode, which is about 1.086 E_{p-p} in domain A. Note that this ratio varies for different high-voltage electrode geometries used in domain B, as will be shown in figure 8.

As an initial condition, homogeneous background ionization with a density of 10^{11} m^{-3} for both electrons and positive ions (N_2^+) is included. All other ion densities are initially zero.

2.4. Afivo AMR framework

The open-source Afivo framework [46] is used in the model to provide AMR for computational efficiency. The refinement criteria are given by

- Refine if $\Delta x > c_0 c_1/\alpha(c_1 E)$,
- De-refine if $\Delta x < \min\{0.125 c_0 c_1/\alpha(c_1 E), d_0\}$,
- $\Delta x \leqslant 1.0$ mm,

where Δx is the grid spacing, which is identical in all directions, and $\alpha(E)$ is the field-dependent ionization coefficient calculated as $S_i/(\mu_e E n_e)$ from equation (4). We use $c_0 = 0.8$ and $c_1 = 1.25$ to balance the refinement ahead and on the sides of the streamer, and $d_0 = 0.1$ mm. The grid has a minimal size of $\Delta x_{min} = 1.8$ μm in the simulations.

The Afivo framework provides a geometric multigrid solver to efficiently solve Poisson's equation (3) and the Helmholtz equation (7). The rod electrode is implemented by modifying the multigrid method with a level-set function [62].

2.5. Definitions

We refer to the moment we apply the high voltage V as $t = 0$ ns. **The streamer position** z_{head} is defined as the axial location at which the electric field has a maximum. **The streamer length** L_s is then computed as $L_s = z_0 - z_{head}$, where z_0 is the axial location of the rod electrode tip. **The streamer velocity** v is computed as the numerical time derivative of the streamer position, measured every 0.5 ns. This causes some fluctuations, so we use a second order Savitzky–Golay filter with a window width of 11 to smooth the velocity.

The head potential $\delta\phi$ is here defined as the potential difference induced by the streamer at its head:

$\delta\phi = \phi(z_{head}, t) - \phi(z_{head}, 0)$, where $\phi(z_{head}, t)$ and $\phi(z_{head}, 0)$ are the actual electric potential and background electric potential at the streamer head, respectively.

The maximal electron drift velocity v_{dmax} is here defined as the electron drift velocity corresponding to the maximal electric field at a particular instant of time.

The background electric field E_{p-p} is here defined as the average electric field between the upper and lower plate electrodes. **The average electric field** E_{r-p} is measured between the rod electrode tip and the grounded electrode.

The breakdown field E_k is defined at which the impact ionization rate is equal to the attachment rate. With our transport data, $E_k = 28$ kV cm^{-1} in air at 300 K and 1 bar.

For a negative streamer fading out in a weak background electric field, **streamer fading** is here arbitrarily defined to occur when the maximal electric field E_{max} decreases to 1.25E_k (35 kV cm^{-1}). Then the streamer position and length at this moment are defined as **the fading position** z_s and **the maximal streamer length** L_{smax}, respectively. We will further discuss the definition of negative streamer fading in section 4.4.

To quantitatively compare with experiments, the streamer diameter d is here defined as the full width at half maximum (FWHM) **optical diameter** $d_{optical}$. We compute the optical diameter from the $N_2(C^3\Pi_u)$ density, which is approximately proportional to the light emission intensity, as most light comes from the $N_2(C^3\Pi_u) \to N_2(B^3\Pi_g)$ transition [63]. First a forward Abel transform is applied [64], after which the emission is vertically integrated to obtain a radial profile, and then the FWHM is determined. A more detailed description is given in [48].

There are actually several different definitions of the streamer diameter, which lead to a different value [52, 65]. To compare different definitions of the streamer diameter, two electrodynamic definitions of the streamer diameter are introduced in appendix A, namely d_{Ez}, related to the decay of the electric field ahead of the streamer, and d_{Er}, related to the location of the maximal radial electric field.

3. Simulation results

In section 3.1, we first present examples of accelerating, steady and fading negative streamers in air. Then we discuss stability fields and steady propagation fields in section 3.2. Next, the dependence of negative streamer fading on the applied voltage is studied in section 3.3. Finally, we investigate steady negative streamers in different background fields in section 3.4.

3.1. Three distinct evolutions of negative streamers

In this section, we investigate negative streamer propagation in domain A, as shown in table 2. Figure 2 shows examples of accelerating, steady and fading negative streamers in air at applied voltages of −162 kV, −146.1 kV and −142 kV, which correspond to background fields (E_{p-p}, see section 2.5) of 12.96 kV cm^{-1}, 11.688 kV cm^{-1} and 11.36 kV cm^{-1}, respectively. Axial profiles corresponding to these cases are shown in figure 3, and their evolutions of the maximal electric
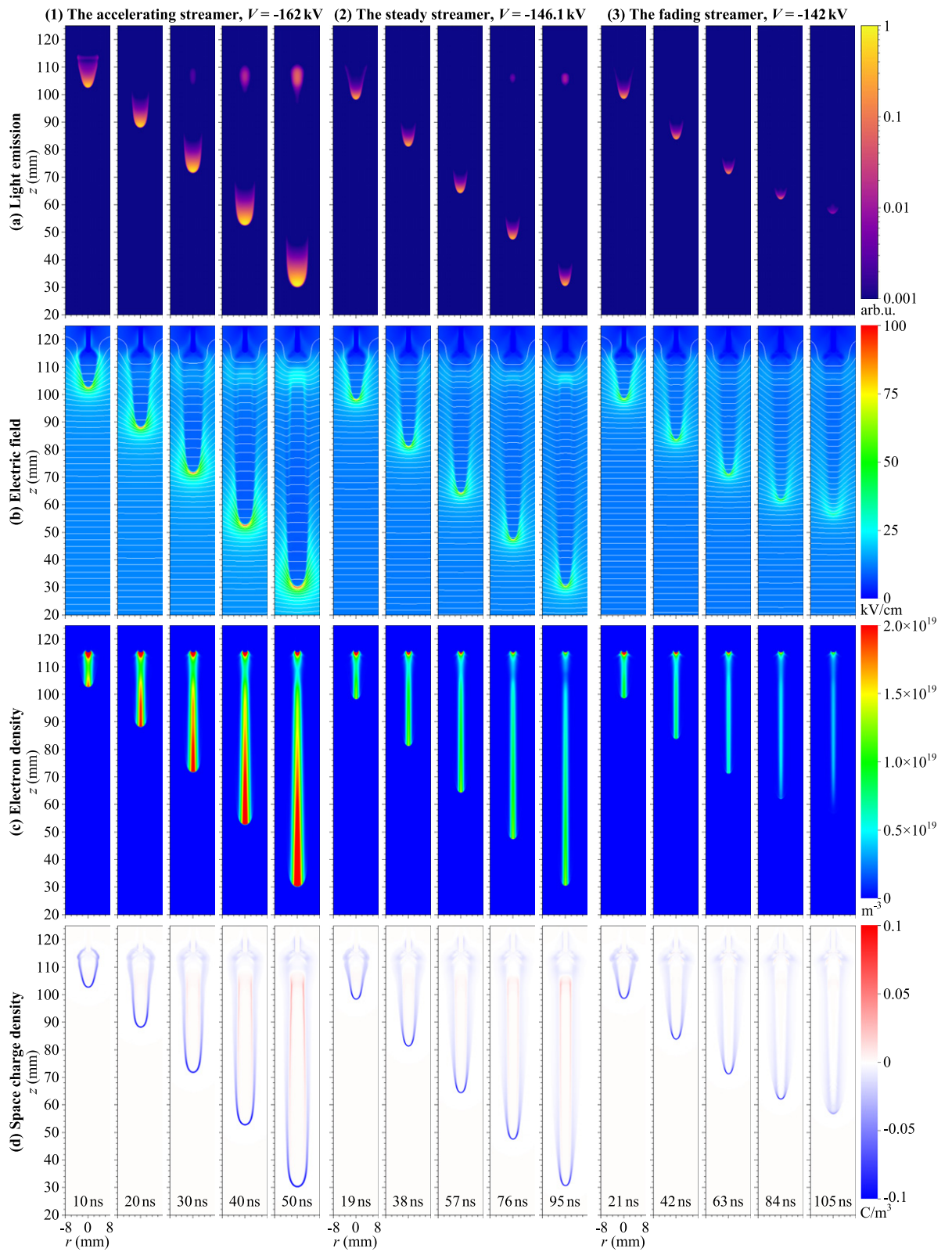
Figure 2. Time evolution of (a) the light emission profile, (b) the electric field E with white equipotential lines, (c) the electron density n_e and (d) the space charge density ρ for (1) accelerating (-162 kV), (2) steady (-146.1 kV) and (3) fading (-142 kV) negative streamers in air. The simulations were performed in domain A until $z_{head} = 30$ mm or fading, see table 2. Light emission was computed with a forward Abel transform, and results are shown using arbitrary units on a logarithmic scale. All panels are zoomed in into the region where $-8 \leqslant r \leqslant 8$ mm and $20 \leqslant z \leqslant 125$ mm.
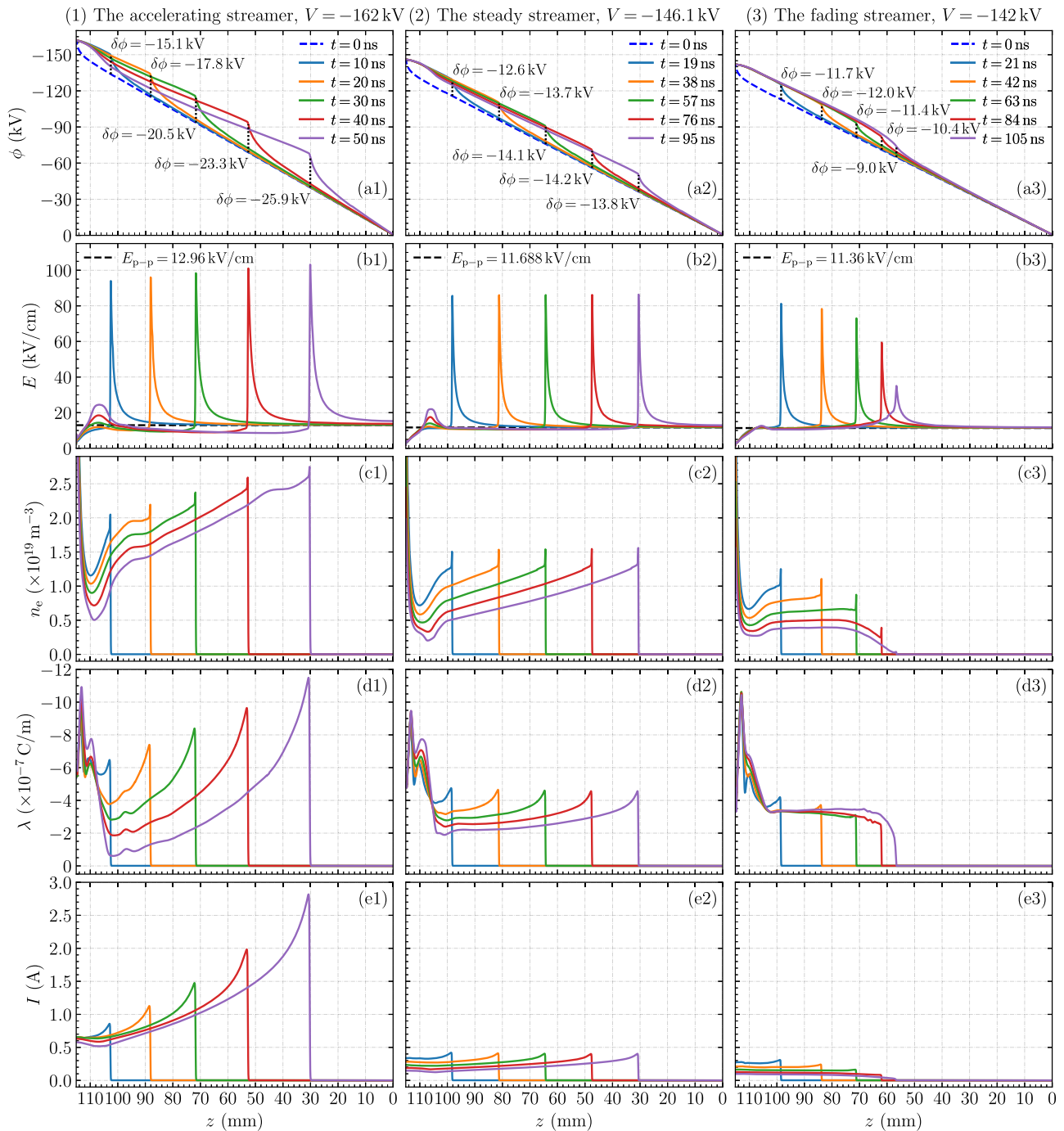
Figure 3. Time evolution of axial profiles, line charge density and electron conduction current for (1) accelerating (-162 kV), (2) steady (-146.1 kV) and (3) fading (-142 kV) negative streamers corresponding to figure 2. The rows show: (a) the on-axis electric potential ϕ and the head potential $\delta\phi$ presented by vertical dotted lines, (b) the on-axis electric field E and the background electric field E_{p-p} presented by dashed lines, (c) the on-axis electron density n_e, (d) the line charge density λ, (e) the electron conduction current I. The quantities λ and I are computed by radially integrating the space charge density ρ and the electron conduction current density ($j = e n_e \mu_e E$) up to $r = 15$ mm. All streamers propagate towards the right.

field, optical diameter and velocity versus the streamer position are shown in figure 4. Several differences can be observed between accelerating, steady and fading negative streamers, which are briefly discussed below.

The accelerating streamer. With an applied voltage of -162 kV the streamer accelerates. Figure 4 shows that the streamer velocity and optical diameter increase almost linearly

with streamer length, which are from about 1.4×10^6 m s^{-1} to 2.4×10^6 m s^{-1} and from about 2.4 mm to 3.6 mm, respectively. In contrast, the maximal electric field is almost constant, with only a slight increase from about 95 kV cm^{-1} to just above 100 kV cm^{-1}. Figure 3 shows that the electron conduction current at the streamer head rapidly increases as the streamer grows, from about 0.9 A to more than 2.5 A. Smaller increases

are visible in the electron density and line charge density at the streamer head, which are from about 2.0×10^{19} m^{-3} to 2.7×10^{19} m^{-3} and from about 6.5×10^{-7} C m^{-1} to 11.5×10^{-7} C m^{-1}, respectively. The streamer head is negatively charged and the streamer tail is positively charged.

The instantaneous light emission profiles resemble the streamer head shape, and the emission intensity increases with growing streamer length. Note that there is also some light emission near the rod electrode.

The electric field inside the streamer channel is lower than the background electric field. As the streamer grows there is a decrease in the internal electric field, to values as low as 8.6 kV cm^{-1} when the streamer head is at $z_{\text{head}} = 30$ mm. This means that the head potential increases from about -15 kV to -26 kV, with the definition shown in section 2.5.

The steady streamer. With a lower applied voltage of -146.1 kV, the streamer propagates with a lower velocity of about 8.9×10^5 m s^{-1} and all streamer properties stay nearly constant during its propagation. Figure 2 shows that the radius of the streamer head is smaller than the channel radius, both for the optical radius and electrodynamic radius, as defined in section 2.5. This steady propagation mode is unstable, as will be shown in section 3.4. It marks the transition between accelerating and decelerating streamers. Quantities such as the maximal electric field, optical diameter, electron density, line charge density, electron conduction current and light emission intensity are all lower than those of the accelerating streamer. However, the internal electric field is higher, namely about 11 kV cm^{-1}. This value can be compared to two definitions of a background field for the steady streamer, which are the background electric field $E_{\text{p}-\text{p}}$ and the average electric field $E_{\text{r}-\text{p}}$ between electrodes, see sections 2.3 and 2.5. First, the background electric field $E_{\text{p}-\text{p}}$ is equal to

$$E_{\text{p}-\text{p}} = |V|/d_{\text{plates}} = 11.688 \text{ kV cm}^{-1}, \tag{9}$$

where $V = -146.1$ kV is the applied voltage and $d_{\text{plates}} = 125$ mm is the distance between two plate electrodes. Second, the average electric field $E_{\text{r}-\text{p}}$ is given by

$$E_{\text{r}-\text{p}} = |V|/(d_{\text{plates}} - L_{\text{rod}}) \approx 12.69 \text{ kV cm}^{-1}, \tag{10}$$

where $L_{\text{rod}} = 9.9$ mm is the length of the rod electrode, as shown in figure 1.

The fading streamer. When the voltage is further reduced to -142 kV, the streamer first decelerates and then fades out. The maximal electric field, electron density and electron conduction current at the streamer head decrease sharply with growing streamer length. The internal electric field behind the streamer head is close to the background electric field of 11.36 kV cm^{-1}. As the streamer grows the head potential decreases from about -12 kV to -9 kV, due to the voltage loss in the streamer channel. The dominant propagation mechanism therefore gradually shifts from ionization to electron drift. This radial outward drift increases the streamer diameter, see figure 4, and it reduces the streamer's maximal electric field and electron density, leading to further deceleration. When the maximal electric field approaches the breakdown field (see section 2.5), the discharge no longer generates significant

ionization and light emission, as shown in figure 2. The velocity is then comparable to the maximal electron drift velocity (see section 2.5), as will be further discussed in section 4.4. The remaining diffuse negative space charge prevents the inception of a new discharge from the high-voltage electrode.

The line charge density in the streamer head slightly decreases as the streamer grows. One way to interpret this is that the electron conduction current in the channel cannot sustain its steady propagation. However, when the streamer has faded, this current leads to an accumulation of negative charge near the streamer head, where the line charge density actually increases. We will further investigate the fading of negative streamers in section 3.3.

3.2. Stability fields and steady propagation fields

To understand whether a streamer is able to propagate in a certain background field, the phenomenological concept of a 'stability field' has commonly been used. There are actually several related definitions of such a stability field. In experiments, the *stability field* E_{st} is usually measured as $|V|/d$, where V is the minimal applied voltage for which streamers can cross a gap of width d [3, 12–14, 37, 38, 40–42, 44, 66]. Values of E_{st} between 10–12.5 kV cm^{-1} for negative streamers in air were found in [10, 14, 18, 43, 67]. The values of $E_{\text{p}-\text{p}}$ (11.688 kV cm^{-1}) and $E_{\text{r}-\text{p}}$ (12.69 kV cm^{-1}) found for the steady propagation case in section 3.1 agree well with these observations.

This concept of a stability field has also been used to estimate the maximal length L_{smax} (see section 2.5) of the streamers that do not cross the gap, using the following empirical equation [68–70]

$$\int_0^{L_{\text{smax}}} (E_{\text{bg}}(z) - E_{\text{st}}) \, \text{d}z = 0, \tag{11}$$

where $E_{\text{bg}}(z)$ denotes the axial background electric field and the path from $z = 0$ to $z = L_{\text{smax}}$ corresponds to the streamer channel. This means that a streamer stops when the average background electric field $\overline{E}_{\text{bg}}$ over the streamer's length is equal to some fixed stability field E_{st}.

The term stability field has also been used for the *steady propagation field* corresponding to steady streamer propagation, as defined in section 1. There have been several numerical studies of such steady propagation. In [26], a negative streamer in air with a constant velocity was found in a background field of about 12.5 kV cm^{-1}. However, in [39], it was argued that such steady propagation fields can lie in a wide range, and steady negative streamers in air were found in background fields from 10 kV cm^{-1} to 28 kV cm^{-1}. In section 3.1, we found a steady propagation field of 11.688 kV cm^{-1} for negative streamers. We will explore the variability of the steady propagation field in section 3.4.

Steady propagation has also been observed for positive streamers in air. In [36], a steady propagation field of 4.675 kV cm^{-1} was found for positive streamers. Later, Li *et al* found steady propagation fields for positive streamers ranging from 4.1 kV cm^{-1} to 5.5 kV cm^{-1} [32]. In [39], a larger range
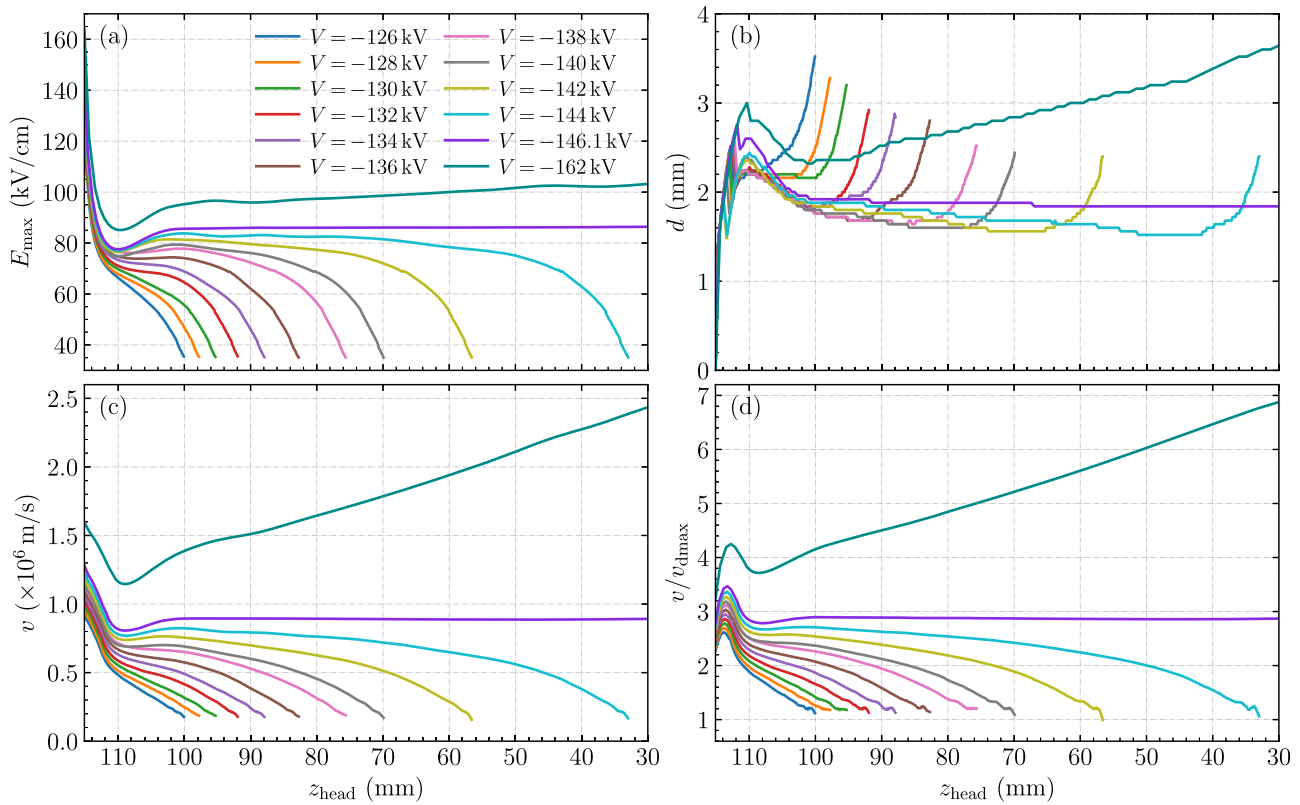
Figure 4. (a) The maximal electric field E_{max}, (b) the optical diameter d, (c) the streamer velocity v and (d) the ratio between streamer velocity and maximal electron drift velocity v/v_{dmax} versus the streamer position z_{head} for negative streamers in air. The simulations were performed in domain A until $z_{head} = 30$ mm or fading, see table 2, with applied voltages from -126 kV to -162 kV. All streamers propagate towards the right.

of steady propagation fields for positive streamers was found, from 4.4 kV cm^{-1} to 20 kV cm^{-1}.

3.3. Dependence of negative streamer fading on the applied voltage

We now investigate the dependence of negative streamer fading on the applied voltage in domain A as well, as shown in table 2. We consider ten applied voltages, evenly spaced between -126 kV and -144 kV. Figure 4 shows the evolution of the maximal electric field, optical diameter, velocity and the ratio between streamer velocity and maximal electron drift velocity for the corresponding streamers until they have just faded, together with the accelerating and steady cases corresponding to figure 2.

With a lower applied voltage, fading occurs earlier. However, the fading negative streamers are otherwise highly similar in terms of the temporal decay of the maximal electric field, velocity, optical diameter and head potential, as well as the spatial decay of the electron density, line charge density and electron conduction current along the streamer direction. Before fading, the optical diameter of fading streamers remains approximately the same as that of the steady streamer. During the fading phase, the streamer head becomes rather diffuse with the optical diameter increasing due to electron drift, and the streamer channel has lost most of conductivity due to attachment. The variation in streamer velocity v is larger than the variation in maximal electron drift velocity v_{dmax},

see section 2.5, so that the variation in their ratio is mostly determined by the streamer velocity. For the steady streamer at $V = -146.1$ kV, the ratio v/v_{dmax} is about 2.87. Note that for the fading streamers, this ratio decreases to about one at the moment of fading. Since they keep propagating, the position of streamer fading and the corresponding maximal streamer length (see section 2.5) depend on some threshold for what is still considered a streamer. We use an arbitrary fading criterion $E_{max} \leqslant 35$ kV cm^{-1}, see section 2.5. If we would use another threshold, for example $E_{max} \leqslant 50$ kV cm^{-1}, this would lead to earlier fading.
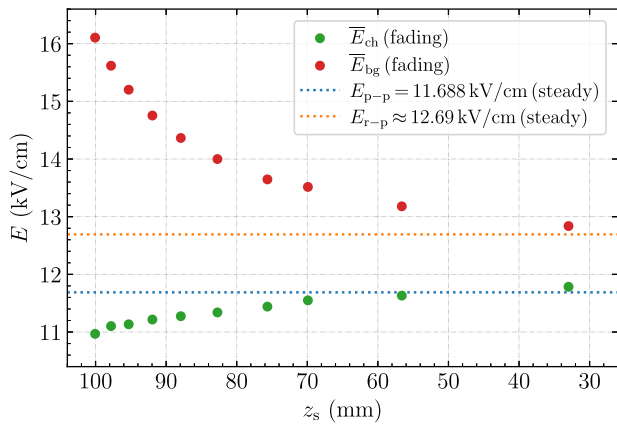
We now look at the average electric field $\overline{E}_{ch}$ and the average background electric field $\overline{E}_{bg}$, both measured along the streamer channel at the moment of fading. These fields are related to the stability field of fading streamers [1, 65, 71, 72]. Figure 5 shows $\overline{E}_{ch}$ and $\overline{E}_{bg}$ for the ten fading cases, as well as the steady case at $V = -146.1$ kV. In general, $\overline{E}_{bg}$ is higher than $\overline{E}_{ch}$. Both $\overline{E}_{ch}$ and $\overline{E}_{bg}$ vary, in particular $\overline{E}_{bg}$ for short streamers. For long streamers, $\overline{E}_{bg}$ decreases to about 12.8 kV cm^{-1}, which is close to the average electric field E_{r-p} of 12.69 kV cm^{-1} corresponding to steady propagation, as given by equation (10). In contrast, $\overline{E}_{ch}$ slightly increases with streamer length and it becomes close to the steady propagation field E_{p-p} of 11.688 kV cm^{-1} corresponding to steady propagation, as given by equation (9). We remark that $\overline{E}_{ch}$ can be related to $\overline{E}_{bg}$ via the head potential $\delta\phi$: $\delta\phi = (\overline{E}_{ch} - \overline{E}_{bg}) \times L_{smax}$.

Figure 5. The average electric field $\overline{E}_{ch}$ and the average background electric field $\overline{E}_{bg}$, both measured along the streamer channel at the moment of fading for the ten fading streamers corresponding to figure 4. The background electric field E_{p-p} and the average electric field E_{r-p} (between rod and plate electrode) for the steady streamer at $V = -146.1$ kV are also shown.
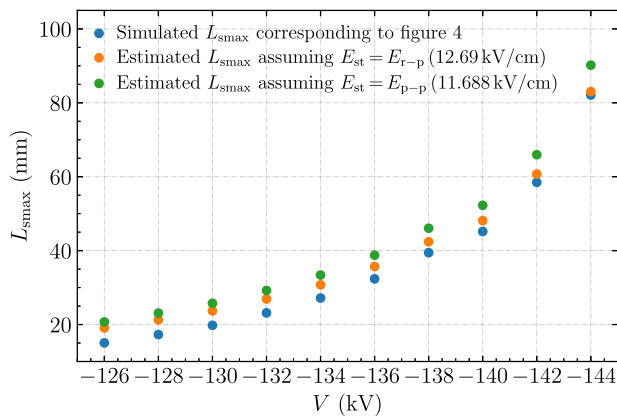

Figure 6. The simulated maximal streamer length L_{smax} versus the applied voltage V for the ten fading streamers corresponding to figure 4. Two estimates based on equation (11) are also presented, by assuming E_{st} is equal to the value of E_{p-p} or E_{r-p} for the steady streamer at $V = -146.1$ kV.

We can estimate the maximal length L_{smax} of fading negative streamers using equation (11), by assuming the stability field E_{st} is equal to the value of E_{p-p} or E_{r-p} for the steady streamer at $V = -146.1$ kV. As shown in figure 6, these estimated maximal lengths are close to—but slightly exceed—the actual maximal lengths. Note that differences depend not only on the value of E_{st}, but also on the threshold used to identify negative streamer fading, and that the relative difference is smaller for longer streamers. Our results confirm that the empirical equation (11) can be used to estimate the maximal streamer length with some fixed conventional stability field.

3.4. Dependence of steady propagation fields on the electrode geometry

In this section, we investigate different steady negative streamers by changing the rod electrode geometry in domain B which has a length of 300 mm, see section 2.3 and table 2. We

consider ten rod electrode lengths L_{rod}, ranging from 3.3 mm to 26.4 mm, with the rod radius given by $L_{rod}/11$.

For each electrode geometry, the applied voltage was varied to find a steady negative streamer. Only one steady solution was found for each electrode. The electron density profiles of these ten steady streamers are shown in figure 7. In figure 8, the streamer velocity, optical diameter and maximal electric field are shown versus the streamer position, as well as the background electric field E_{p-p} and the average electric field E_{r-p}. Note that all streamer properties remain essentially constant. With a longer rod electrode, the steady streamer propagates faster, and the optical diameter and maximal electric field are also higher, but the required background electric field is lower.

The relationships between streamer properties and the optical diameter for these steady streamers are further illustrated in figure 9. The streamer velocity and head potential have approximately linear relationships with the optical diameter.

Axial profiles corresponding to these steady streamers at $z_{head} = 100$ mm are also shown in figure 10. Here the line conductivity σ^* was integrated radially as

$$\sigma^*(z) = 2\pi e \int_0^{r_{max}} r n_e \mu_e \, dr, \qquad (12)$$

where e is the elementary charge and r_{max} is a few times larger than the streamer radius.

For these ten rod electrodes, the background electric field E_{p-p} ranges from 9.19 kV cm^{-1} to 15.75 kV cm^{-1} for L_{rod} from 26.4 mm to 3.3 mm. Typical values range from 10 kV cm^{-1} to 12.5 kV cm^{-1}, but for short electrodes the required E_{p-p} rapidly increases. We could not simulate steady streamers for longer or shorter rod electrodes in domain B, due to branching for longer electrodes and due to the difficulty in locating the steady regime for shorter electrodes.

As was discussed in section 3.2, E_{p-p} is closely related to the steady propagation field. Our results therefore confirm the conclusion in [39] that steady propagation fields can lie in a wide range, depending not only on the gas but also on the streamer's properties. Since streamer properties are determined by many factors, including e.g., the electrode geometry, the applied voltage waveform and initial conditions, this explains part of the spread in experimentally measured stability fields [38, 40–44].

That a longer electrode requires a lower E_{p-p} for steady propagation is in agreement with the results for steady positive streamers in [32]. In [32], it was argued that the length over which a streamer has a significant conductivity depends on the product $v\tau$, where v is the streamer velocity and τ a characteristic time scale for the loss of conductivity due to e.g., attachment. With a longer electrode, a faster streamer emerges, which will therefore have a longer conductive length, so that a lower background field is sufficient for its field enhancement, as can be seen in figures 7 and 10.

Figure 11 shows the time evolution of axial profiles for the steady streamer with $L_{rod} = 3.3$ mm. As can be seen in figures 7 and 11, the conductive length is short enough to cause the internal field in the back of the streamer channel to return to its background field of 15.75 kV cm^{-1}. Like for steady positive streamers [32, 36], steady negative streamers
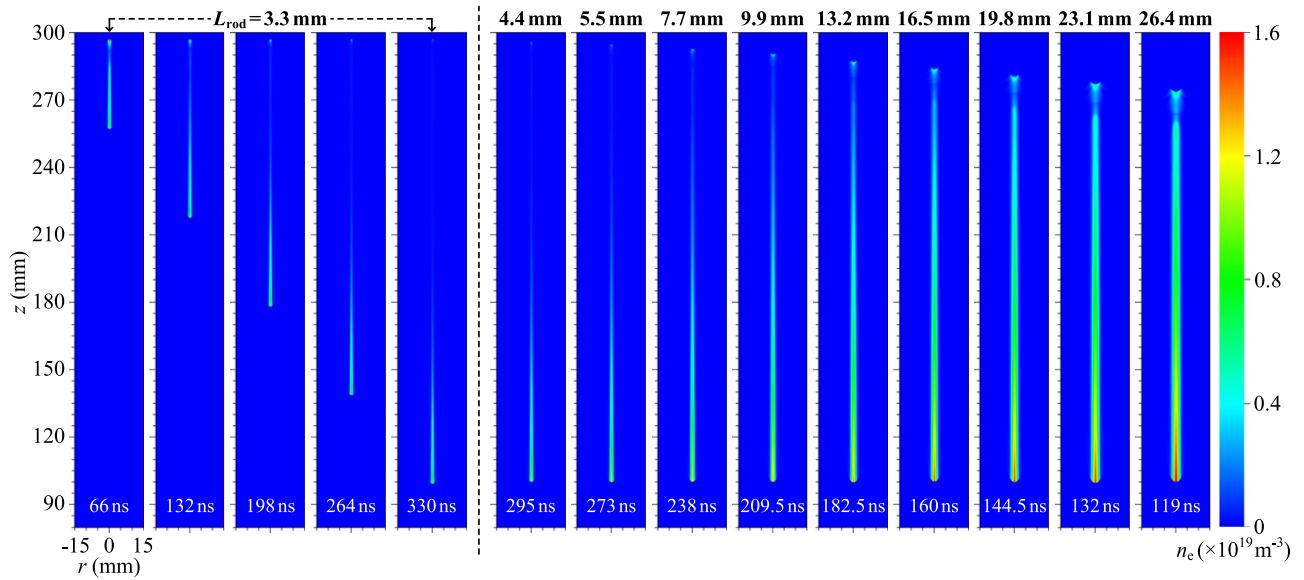
Figure 7. The electron density n_e for ten steady negative streamers in air with different rod electrode lengths L_{rod} from 3.3 mm to 26.4 mm. The simulations were performed in domain B until the streamer reached $z_{head} = 100$ mm, see table 2. The time evolution of n_e for the case of $L_{rod} = 3.3$ mm is shown on the left. On the right, n_e is shown for the remaining nine steady streamers at $z_{head} = 100$ mm.
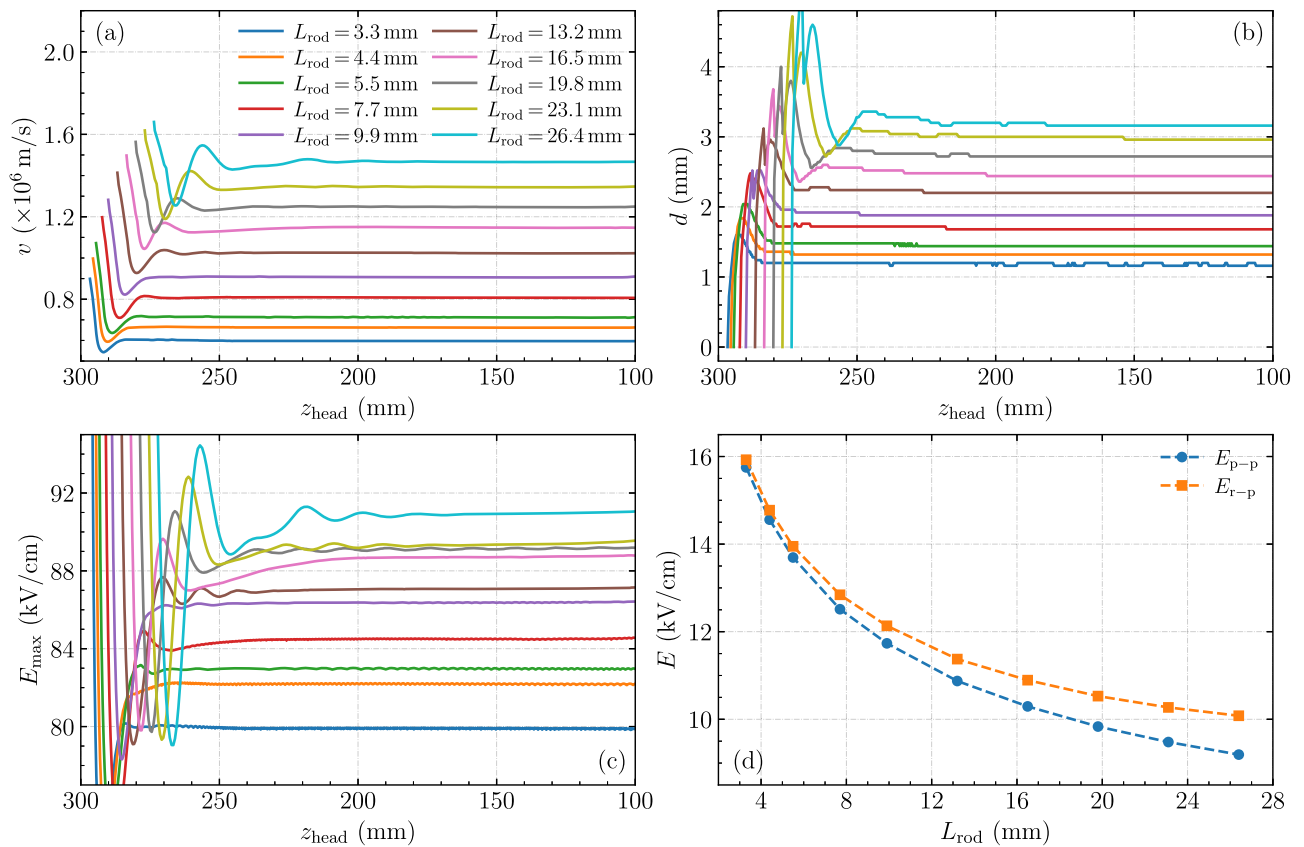

Figure 8. (a) The streamer velocity v, (b) the optical diameter d, and (c) the maximal electric field E_{max} versus the streamer position z_{head} for the ten steady streamers corresponding to figure 7. The corresponding background electric field E_{p-p} and the average electric field E_{r-p} between rod and plate electrode are shown in panel (d) versus the rod electrode length L_{rod}. All streamers propagate towards the right.

do not require a conductive channel to sustain the propagation, as will be discussed in section 4.1. The electric field in the streamer channel ranges from about 14 kV cm^{-1} to E_{p-p} and

the attachment time ranges from 35–50 ns, which coincidentally agrees well with the electron loss times for steady positive streamers in air [32, 36]. However, the streamer velocity of
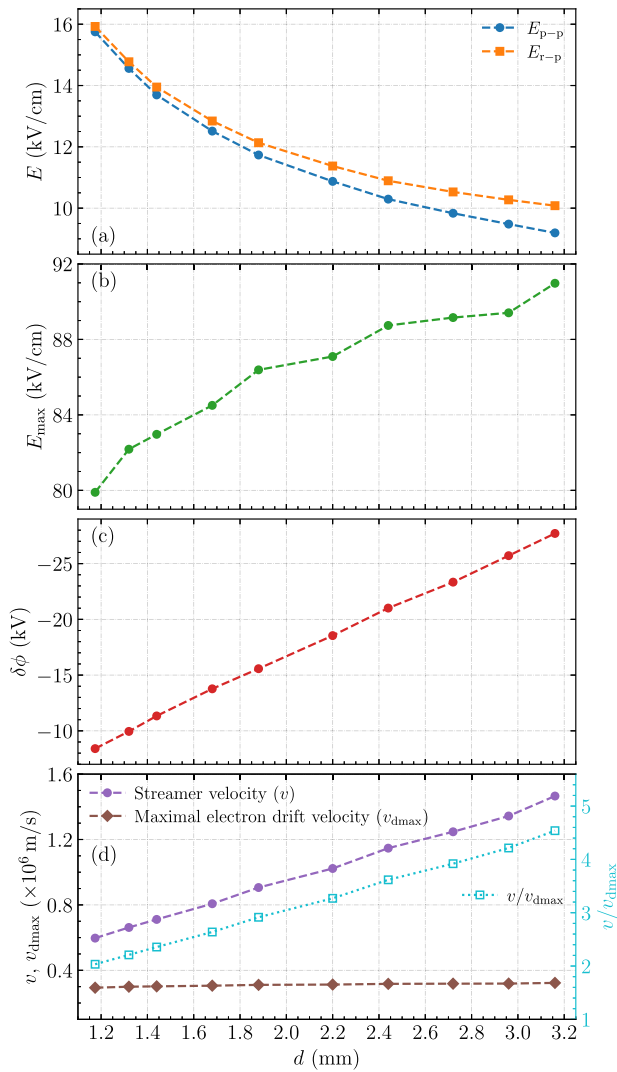
Figure 9. (a) The background electric field E_{p-p} and the average electric field E_{r-p}, (b) the maximal electric field E_{max}, (c) the head potential $\delta\phi$ and (d) the streamer velocity v, maximal electron drift velocity v_{dmax} and their ratio v/v_{dmax} versus the optical diameter d for the ten steady streamers corresponding to figure 7. Each symbol in panels (b)–(d) represents one steady streamer, by taking an average over the propagation from $z_{head} = 150$ mm to $z_{head} = 100$ mm.

Figure 10. (a) The on-axis electric field E and the background electric field E_{p-p}, (b) the on-axis electron density n_e, (c) the line conductivity σ^* and (d) the electron conduction current I for the ten steady streamers at $z_{head} = 100$ mm corresponding to figure 7. All streamers propagate towards the right.

about 6×10^5 m s^{-1} in figure 11 is much larger than that of steady positive streamers (about 0.3–1.2×10^5 m s^{-1}), which leads to a longer conductive length. Another difference is that the electron density contains an overshoot near the head of negative streamers, as can be seen in figures 3(c1)–(c3), 10(b) and 11(b).

We remark that the steady streamers are unstable, in the sense that a tiny change in the applied voltage causes them to either accelerate or decelerate. This instability is illustrated in figure 12, which shows streamer velocity versus position for cases with applied voltages that differ by ±1 kV from the steady values. With these different applied voltages, the streamer continually accelerates or decelerates. Hence, the steady streamer is not really stable, but exists
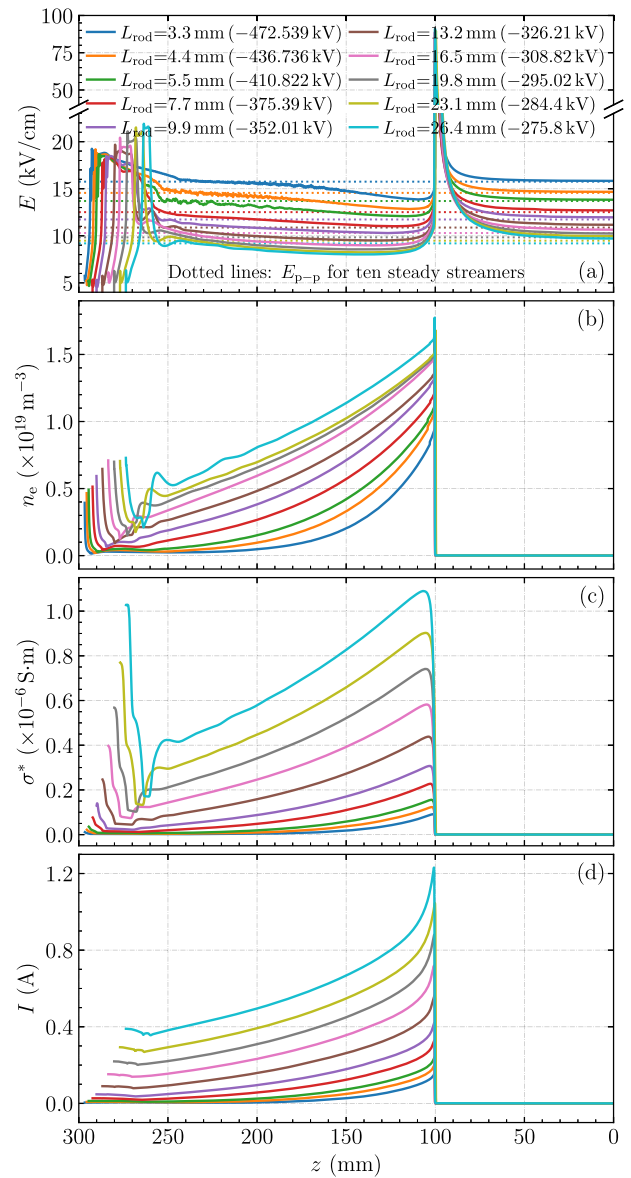
only at the unstable boundary between accelerating and fading streamers. Any minor change in input data or numerical parameters would also lead the steady streamer to eventually accelerate or decelerate. The results in figure 12 indicate that this instability is stronger for a slower negative steady streamer.

4. Discussion and analysis

Below, we discuss several important questions about negative streamers in air, and compare their properties with those of positive streamers.
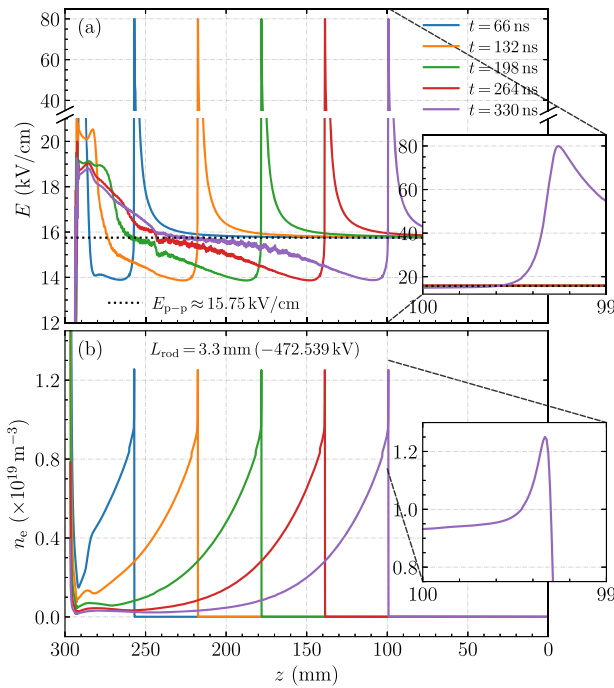
Figure 11. Time evolution of (a) the electric field E and (b) the electron density n_e along z axis for the steady streamer with $L_{rod} = 3.3$ mm from figure 7. The background field $E_{p-p} \approx 15.75$ kV cm^{-1} is shown in panel (a) for comparison. Zoomed views of E and n_e at $t = 330$ ns and 99 mm $\leqslant z \leqslant 100$ mm are included, revealing an overshoot in n_e in the streamer head.
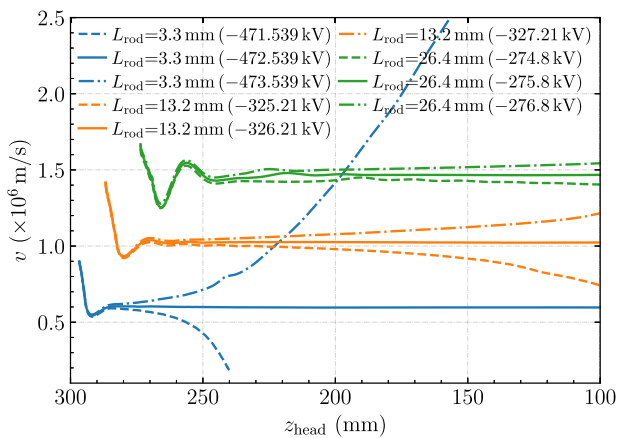

Figure 12. Illustration of the instability of steady negative streamers. The streamer velocity v is shown versus the streamer position z_{head} for steady streamers with $L_{rod} = 3.3$ mm, 13.2 mm and 26.4 mm, together with cases in which the applied voltages differ by ± 1 kV from the respective steady values. All streamers propagate towards the right.

4.1. Does a negative streamer require a conductive channel to sustain its propagation?

A key difference between negative and positive streamers is that negative streamers propagate in the same direction as the electron drift velocity, whereas positive streamers propagate opposite to it. This means that positive streamers 'suck up'

free electrons ahead of them, a bit like a vacuum cleaner, which come out at the back of the streamers. In contrast, a negative streamer 'emits' electrons in the forward direction, figuratively speaking like a garden hose. The excess of these electrons (compared to the positive ion density) forms the negative charge layer that provides field enhancement.

In case of steady propagation, which is an unstable mode, the net charge in the streamer head region is conserved. The electric field, modified by the streamer, is then such that the net charge simply translates, while ionization is created at the streamer tip and lost at its back. A negative streamer therefore does not require a conductive channel in order to sustain its propagation, as shown in figure 7. The same observation was recently made for positive streamers in [36], which were referred to as 'solitary streamers'.

Furthermore, our results show that an accelerating negative streamer also does not require a conductive channel connected to an electrode. In such streamers, the head charge increases over time, but this head charge can be supplied by polarizing the channel behind the streamer.

4.2. Is there a minimal steady negative streamer?

For positive streamers, the concept of a minimal streamer, with a certain minimal diameter d_{min}, was postulated in [73]. In the experiments of [74], a relation $p \cdot d_{min} = 0.20 \pm 0.02$ mm bar for the minimal optical diameter was found in air at room temperature, at pressures from 0.013 to 1 bar. In nitrogen, streamers were found to be thinner, with $p \cdot d_{min} = 0.12 \pm 0.03$ mm bar. By improving gas purity and optical diagnostics, similar trends but with somewhat lower values of $p \cdot d_{min}$, namely 0.12 mm bar for air and 0.07 mm bar for nitrogen, were found in [75]. Furthermore, in the theoretical and numerical study of [29], the minimal optical diameters of positive streamers in air at atmospheric pressure were related to E_{max}. For $E_{max} = 140$ kV cm^{-1} and 160 kV cm^{-1}, minimal diameters of 0.27 mm and 0.20 mm were respectively predicted, in the limit of zero streamer velocity. In [39], steady propagation for both positive and negative streamers in air at atmospheric pressure was simulated. Smaller minimal diameters of 0.072 mm for positive streamers and of about 0.5 mm for negative streamers were suggested, where the diameter was defined as the FWHM of the electron density.

In another numerical study of [14], a minimal electrodynamic diameter (d_{Er}, see appendix A) of about 1.3 mm in air at atmospheric pressure was observed for negative streamers. Experimentally, few measurements appear to be available for minimal negative streamer diameters. In [13], the negative streamer with a minimal optical diameter of 1.2 mm was observed in air at 1 bar. However, negative streamer inception required a rather high applied voltage in the above two studies, and thinner negative streamers could be generated with a different electrode geometry and applied voltage waveform.

From our simulations, we can estimate a lower bound for the minimal optical diameter of steady negative streamers in air. The variation of their optical diameter d in different background fields is shown in figure 9. The streamer optical diameter has approximately linear relationships with several

quantities: the streamer velocity v, the ratio between streamer velocity and maximal electron drift velocity v/v_{dmax}, and the head potential $\delta\phi$, as shown in figure 13. These linear relationships can be described by

$$v(d) = 4.28 \times 10^8 d + 9.41 \times 10^4, \tag{13}$$

$$v(d)/v_{\mathrm{dmax}}(d) = 1.24 \times 10^3 d + 0.56, \tag{14}$$

$$\delta\phi(d) = -9.60 \times 10^6 d + 2.59 \times 10^3, \tag{15}$$

where all above quantities have for simplicity of notation been divided by their respective units (using metres, seconds and volts). Based on these relations, rough estimates can be made for a lower bound on the minimal optical diameter d_{min}:

- The diameter at which $v = v_{\mathrm{dmax}}$, which gives $d_{\mathrm{min}} = 0.35$ mm.
- The diameter at which $\delta\phi = 0$, which gives $d_{\mathrm{min}} = 0.27$ mm. Note that in this theoretical limit there is essentially no space charge, and thus no light emission to deduce an optical diameter from.

So for the minimal optical diameter, these rough lower bounds give 0.27 mm to 0.35 mm, smaller but comparable to the measured minimal optical diameter of 1.2 mm found in [13].

4.3. The ratio between streamer velocity and electron drift velocity

For negative streamers, the ratio between streamer velocity and maximal electron drift velocity v/v_{dmax} should be greater than one [1, 34, 76]. In our simulations, v/v_{dmax} ranges from about 2.0 to 4.5 for steady negative streamers. In contrast, this ratio was observed to be about 0.05 to 0.26 for steady positive streamers in [32]. To understand why these ratios are so different for steady negative and positive streamers, it is useful to consider an analytic approximation for uniformly translating streamers, as was done in [29]. If we assume that $\nabla \cdot (\mu_{\mathrm{e}} \mathbf{E} n_{\mathrm{e}}) \approx \mu_{\mathrm{e}} \mathbf{E} \cdot \nabla n_{\mathrm{e}}$ (i.e., μ_{e} is assumed constant and $\nabla \cdot \mathbf{E} = 0$), and if we ignore effects due to diffusion and photoionization, we can derive the following expression

$$-\frac{v}{v_{\mathrm{d}}} \frac{\partial_z n_{\mathrm{e}}}{n_{\mathrm{e}}} \pm \frac{\partial_z n_{\mathrm{e}}}{n_{\mathrm{e}}} = \bar{\alpha}, \tag{16}$$

where v is the streamer velocity (in the $+z$ direction), $v_{\mathrm{d}} = |\mu_{\mathrm{e}} E|$ the absolute value of the electron drift velocity, $\bar{\alpha}$ the effective ionization coefficient, and the $+$ sign corresponds to negative streamers and the $-$ sign to positive ones. If we introduce the length scale $\lambda_{n_{\mathrm{e}}} = n_{\mathrm{e}}/|\partial_z n_{\mathrm{e}}|$ and consider the fact that $\partial_z n_{\mathrm{e}}$ is negative for a streamer propagating in the $+z$ direction, equation (16) can be written as

$$|v|/v_{\mathrm{d}} = \bar{\alpha}\lambda_{n_{\mathrm{e}}} \pm 1, \tag{17}$$

with the $+$ sign corresponding to negative streamers and the $-$ sign to positive ones. Note that v is assumed constant here, whereas v_{d}, $\bar{\alpha}$ and $\lambda_{n_{\mathrm{e}}}$ all vary ahead of a streamer.

Even without knowing the values of $\bar{\alpha}$ and $\lambda_{n_{\mathrm{e}}}$, a couple of statements can be made about the ratio v/v_{dmax}. First, for
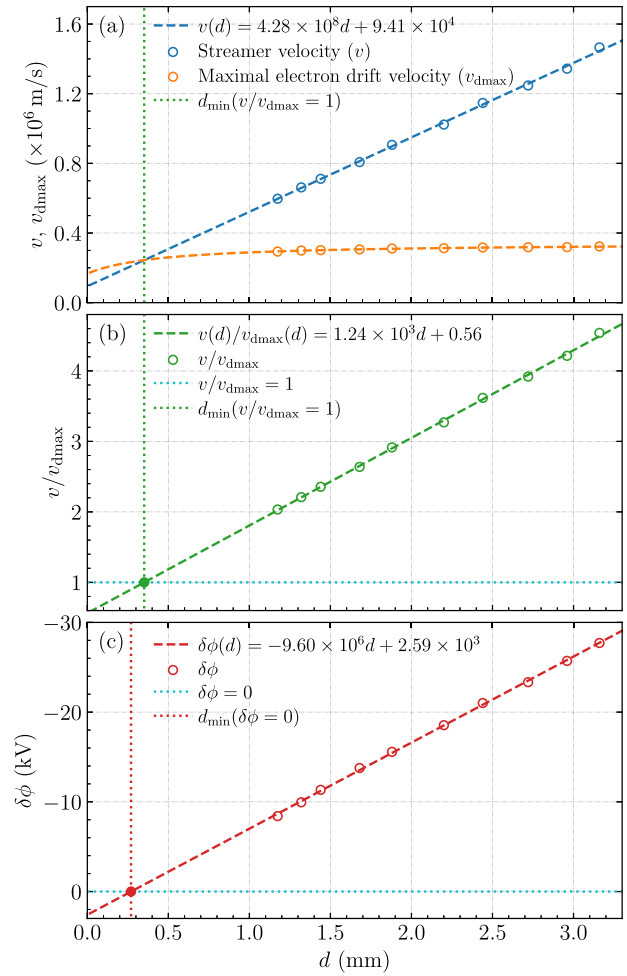

Figure 13. Linear relationships between the optical streamer diameter d and (a) the streamer velocity v, (b) the ratio v/v_{dmax} and (c) the head potential $\delta\phi$, respectively. The maximal electron drift velocity v_{dmax} is also shown in panel (a). The open circles ∘ correspond to the steady cases shown in figure 7. Estimates of a minimal optical diameter d_{min} for the steady streamers are indicated by full circles ●. These estimates are given by: (b) the diameter at which $v/v_{\mathrm{dmax}} \approx 1$ and (c) the diameter at which $\delta\phi = 0$.

steady positive streamers, v/v_{dmax} can in principle be arbitrarily small, in agreement with the value of 0.05 mentioned above. The limit of zero streamer velocity corresponds to $\lambda_{n_{\mathrm{e}}} = 1/\bar{\alpha}$, and thus a density profile proportional to $\exp\left(-\int \bar{\alpha} \, \mathrm{d}z\right)$. On the other hand, for steady negative streamers, v/v_{dmax} cannot be lower than one, as expected. In high background fields streamers usually accelerate, but if their properties do not change rapidly, equation (17) is still approximately valid. The fact that negative and positive streamers become similar in high background fields [13, 14, 26] therefore suggests that the term $\bar{\alpha}\lambda_{n_{\mathrm{e}}}$ then becomes large.

If we hypothetically assume that a steady positive and negative streamer exist with the same values of $\bar{\alpha}$ and $\lambda_{n_{\mathrm{e}}}$, then equation (17) implies that $v/v_{\mathrm{dmax}} \geqslant 2$ for the steady negative streamer, since this ratio cannot be negative for the steady positive streamer. However, $\bar{\alpha}$ and $\lambda_{n_{\mathrm{e}}}$ are generally different for positive and negative streamers. In simulations in another computational domain, which are not presented here, we have

Table 3. Comparison between steady negative and positive streamers, corresponding to the lowest and highest respective background electric fields. For the steady negative streamers, properties were obtained at the moment corresponding to figure 10, and for the positive ones they were obtained from [32].

Quantity	Lowest background field			Highest background field		
	Negative	Positive	Ratio	Negative	Positive	Ratio
v (m s^{-1})	1.47×10^6	1.2×10^5	12.25	5.97×10^5	3×10^4	19.90
R_{Er} (mm)a	3.15	0.11	28.64	1.25	0.036	34.72
$E_{\mathrm{p-p}}$ (kV cm^{-1})	9.19	4.05	2.27	15.75	5.42	2.91
$E_{\max}$ (kV cm^{-1})	91	152	0.60	80	222	0.36
$E_{\min}$ (kV cm^{-1})b	8.02	1.17	6.85	13.87	0.42	33.02
$\max(n_e)$ (m^{-3})	1.77×10^{19}	1.11×10^{20}	0.16	1.25×10^{19}	3.12×10^{20}	0.04
$\max(n_i^+)$ (m^{-3})c	1.68×10^{19}	1.13×10^{20}	0.15	1.00×10^{19}	3.30×10^{20}	0.03
$I_{\max}$ (A)	1.23	1.38×10^{-2}	89.13	0.16	1.91×10^{-3}	83.77
$\lambda_{\max}$ (C m^{-1})	-8.41×10^{-7}	1.11×10^{-7}	-7.58	-2.71×10^{-7}	5.44×10^{-8}	-4.98
$\sigma_{\max}^*$ (S m)	1.09×10^{-6}	5.09×10^{-8}	21.41	9.13×10^{-8}	2.38×10^{-8}	3.84
v_{dmax} (m s^{-1})	3.23×10^5	4.7×10^5	0.69	2.94×10^5	6.1×10^5	0.48
v/v_{dmax}	4.55	0.26	17.50	2.03	0.049	41.43
$\delta\phi$ (kV)	-27.61	2.83	-9.42	-8.37	1.52	-5.51

aR_{Er} is the electrodynamic radius at which the radial electric field has a maximum, see appendix A.
b$E_{\min}$ is the minimal internal on-axis electric field behind the streamer head.
cn_i^+ is the total number density of all positive ion species.

actually found steady negative streamers for which v/v_{dmax} could be as low as 1.8. Note that without photoionization and background ionization, the ratio v/v_{dmax} is expected to be close to one [77].

4.4. The definition of negative streamer fading

When the background electric field is too low to sustain steady propagation, a negative streamer fades out and loses its field enhancement, and the streamer velocity becomes comparable to the maximal electron drift velocity. However, the discharge does not fully stop at some point, because the electrons that make up its space charge layer continue their drift motion, further lowering the velocity and field enhancement. This makes it hard to uniquely define when a negative streamer has faded. For the results presented in sections 3.1 and 3.3, we have somewhat arbitrarily used the criterion $E_{\max} \leqslant 35\,\mathrm{kV\,cm}^{-1}$. A related criterion could for example be

$$E_{\max}/\alpha(E_{\max}) \geqslant V_c,$$

where V_c is for example 250 V. Note that $eE/\alpha(E)$, where e is the elementary charge, can be interpreted as the energy an electron has to gain from the field per ionization.

We can also consider the ratio between streamer velocity and maximal electron drift velocity v/v_{dmax}. As was discussed in section 4.3, a negative streamer needs to propagate with at least the maximal electron drift velocity. Our results in figure 4 suggest that a criterion like $v/v_{\mathrm{dmax}} \leqslant \kappa$, with for example $\kappa = 1.5$, could be used to define the moment of negative streamer fading.

However, it was argued in [39] that for steady negative streamers $E_{\max}$ can be as weak as $\sim 1.2E_k$, and that the ratio v/v_{dmax} can be as low as ~ 1.03. If that is the case, it is hard to distinguish between a fading negative streamer and an electron avalanche with weak field enhancement.

Finally, we remark that negative streamer fading differs significantly from positive streamer stagnation. When positive streamers stagnate, their field enhancement tends to increase [31, 32]. Only after their velocity has become comparable to the ion drift velocity, which is much lower than the electron drift velocity, do they lose their field enhancement.

4.5. Comparison between steady negative and positive streamers

We can quantitatively compare our simulated steady negative streamers with the results for steady positive streamers in [32]. We consider the steady negative and positive cases corresponding to the lowest and highest respective background electric fields, and several properties of these streamers are compared in table 3. Velocity, radius, ratio between streamer velocity and maximal electron drift velocity and the maximal electron conduction current all differ by more than an order of magnitude between these steady negative and positive streamers. Due to their higher velocities, the conductive lengths of the two steady negative streamers are respectively significantly longer than that of the positive steady ones.

Given these major differences, it is perhaps a bit surprising that the steady propagation fields for these negative and positive cases differ by a much smaller factor.

Estimation of the internal field. We now compare the steady negative and positive streamers from the point of view of their electron conduction current, line charge density, line conductivity and internal electric field. If a streamer translates approximately uniformly with velocity v, its line charge density λ should translate approximately uniformly with the same velocity. The evolution of λ is then given by $\partial_t \lambda = -\partial_x I = -v\partial_x \lambda$, where I is the electron conduction current and v is the streamer velocity. General solutions are the
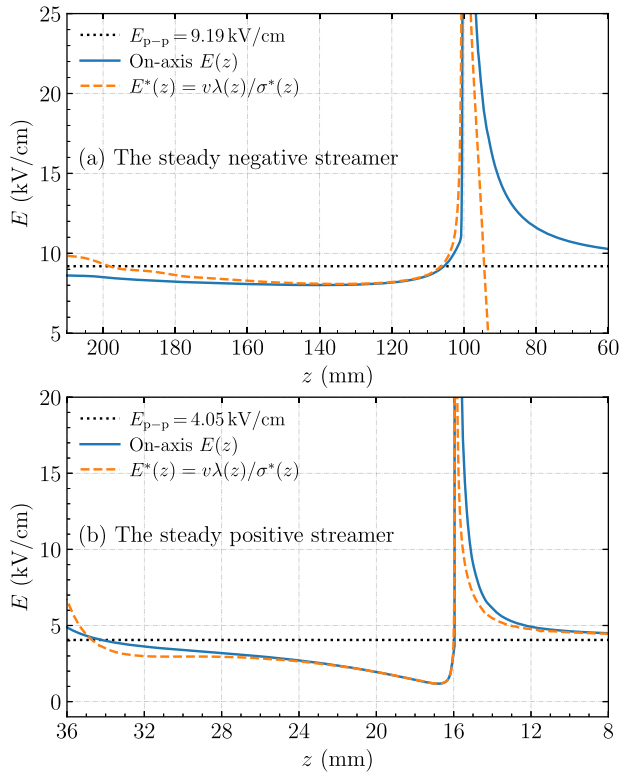
Figure 14. The average electric field $E^*(z)$ in the z direction according to equation (20), together with the actual on-axis electric field $E(z)$ for steady negative and positive streamers from table 3 corresponding to the lowest background fields. Both streamers propagate towards the right.

form $I(z) = v\lambda(z) + I_0$, but since there is no current ahead of the streamer, $I_0 = 0$, and

$$I(z) = v\lambda(z). \tag{18}$$

On the other hand, we can also write the current as

$$I(z) = \sigma^*(z)E^*(z), \tag{19}$$

where $\sigma^*(z)$ is the streamer's line conductivity given by equation (12) and $E^*(z)$ is the average electric field in the z direction. If equations (18) and (19) are combined, the result is

$$E^*(z) = v\lambda(z)/\sigma^*(z). \tag{20}$$

Figure 14 shows the actual on-axis electric field for the positive and negative steady streamers from table 3 corresponding to the lowest background fields, together with results from equation (20). Behind the streamer head, $E^*(z)$ agrees well with the on-axis electric field $E(z)$ for both steady streamers. Note that discrepancies are visible ahead of the streamer, where equation (20) does not apply.

The minimal internal on-axis electric fields E_{min} behind the streamer head are 8.02 kV cm^{-1} and 1.17 kV cm^{-1} for the above-mentioned steady negative and positive streamers, respectively. These internal fields are related to the steady propagation fields, which they cannot exceed. There is however a polarity difference. For steady positive streamers, the internal field can be significantly below the background field

[32], whereas for steady negative streamers these fields are rather similar. In other words, the screening of the electric field is weaker for steady negative streamers.

Our observations of steady negative streamers can be related to equation (20) as follows. We find a lower steady propagation field for a faster steady streamer, which also has a higher line charge density λ. Equation (20) suggests that this can only be the case when the line conductivity σ^* increases more rapidly than the product $v\lambda$, which is primarily driven by an increase in the radius.

5. Conclusions and outlook

5.1. Conclusions

We have simulated single negative streamers in air at 300 K and 1 bar in 125 mm and 300 mm long gaps, using a 2D axisymmetric fluid model. With the same initial conditions, accelerating, steady and fading negative streamers were obtained by changing the background electric field. The properties of the steady streamers remained nearly constant during their propagation. However, this steady propagation mode is not stable, in the sense that a small change in parameters or streamer properties causes them to accelerate or decelerate. Our main conclusions are listed below:

- With different high-voltage electrode geometries, steady propagation for negative streamers was obtained in background fields ranging from 9.19 kV cm^{-1} to 15.75 kV cm^{-1}. The lowest background field was obtained for the longest electrode and the fastest steady streamer. This confirms that there is no unique steady propagation field (or stability field) for such streamers, as was previously suggested in [39] and as was recently found for positive streamers [32].

- Steady negative streamers are able to keep propagating over tens of centimeters with only a finite conductive length behind their heads, similar to steady positive streamers [32, 36]. They transport a constant amount of charge, and their propagation resembles a solitary wave. The conductivity in the back of the streamer channel disappears mainly due to attachment.

- The ratio between streamer velocity and maximal electron drift velocity v/v_{dmax} for steady negative streamers is much higher than that of steady positive streamers. For steady positive streamers, v/v_{dmax} can be as small as 0.05 [32]. In contrast, for steady negative streamers, v/v_{dmax} cannot be lower than one, and the minimum ratio we observe is two.

- When we compare the steady negative and positive streamers corresponding to the lowest and highest respective background fields, their properties are totally different. The velocity, radius, v/v_{dmax}, and maximal electron conduction current all differ by more than an order of magnitude. In contrast, the lowest steady propagation fields of 9.19 kV cm^{-1} (negative) and 4.05 kV cm^{-1} (positive) differ only by a factor of about two.

- For steady negative streamers, we observe approximately linear relationships between the optical diameter and the streamer velocity, the steamer head potential and the ratio v/v_{dmax}. From these linear relations, rough estimates can be made for a lower bound on the minimal optical diameter, which lie between 0.27 mm and 0.35 mm.

In addition, we have the following minor conclusions:

- In different background fields, negative streamer fading is highly similar, although fading occurs earlier in a lower background field. The channel conductivity disappears, and the ratio v/v_{dmax} decreases to about one.
- It is hard to uniquely define when a negative streamer has faded. We have proposed several criteria, based on e.g., the maximal electric field or the ratio v/v_{dmax}.
- There are different definitions of the streamer diameter. The electrodynamic diameter is usually larger than the optical diameter, with an approximately constant ratio of about two between them for steady negative streamers.

5.2. Outlook

An interesting question for future work would be how the steady propagation field depends on e.g., the applied voltage waveform and the initial conditions. Understanding the relationships that were observed between several streamer properties requires further analysis as well. Finally, future research could implement more realistic boundary conditions on the high-voltage electrode, for example, by including electron emission, to more realistically study the inception of negative streamers.

Acknowledgments

Data availability statement

The data that support the findings of this study are openly available at the following URL/DOI: https://doi.org/10.5281/zenodo.6400856.

Appendix A. Diameter comparison

In addition to the optical diameter d_{optical} defined in section 2.5, we here give two other definitions of the streamer diameter. First, there is the electrodynamic diameter $d_{Ez} = 2 \times R_{Ez}$, based on the decay of the on-axis electric field ahead of the streamer head. Near the head, this field decay is approximately quadratic, like that of a charged sphere, which depends on the
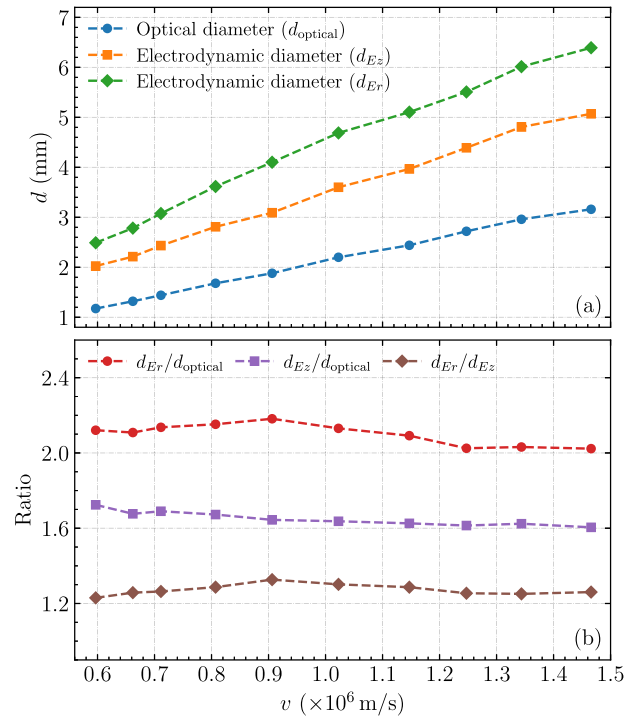

Figure A1. (a) The optical diameter d_{optical}, the electrodynamic diameter d_{Ez} and the electrodynamic diameter d_{Er} versus the streamer velocity v for the ten steady streamers corresponding to figure 7. Each symbol represents one case, by taking an average over the propagation from $z_{\text{head}} = 150$ mm to $z_{\text{head}} = 100$ mm. (b) The ratios of $d_{Er}/d_{\text{optical}}$, $d_{Ez}/d_{\text{optical}}$ and d_{Er}/d_{Ez} versus the streamer velocity v.

streamer radius. Ahead of the streamer ($z > z_{\text{head}}$), it can be approximated by:

$$E_{\text{fit}}(z) = E_{\text{bg}} + (E_{\text{max}} - E_{\text{bg}})\left(1 + \frac{z - z_{\text{head}}}{R_{Ez}}\right)^{-2}, \quad \text{(A.1)}$$

where E_{bg} is the axial background electric field and E_{max} is the maximal electric field at the streamer head. Since E_{bg} and E_{max} are known, we can obtain the radius R_{Ez} by locating the z coordinate at which the actual electric field is equal to $0.25E_{\text{max}} + 0.75E_{\text{bg}}$, which corresponds to $E_{\text{fit}}(z_{\text{head}} + R_{Ez})$. Second, there is the electrodynamic diameter $d_{Er} = 2 \times R_{Er}$, where R_{Er} is the radius at which the radial component of the electric field E_r has a maximum [32, 49, 57, 78].

Figure A1 shows these three definitions of the streamer diameter for the cases shown in figure 7, as well as the ratios between them. The ratios of $d_{Er}/d_{\text{optical}}$, $d_{Ez}/d_{\text{optical}}$ and d_{Er}/d_{Ez} are approximately constant, and their values are about 2.1, 1.6 and 1.3, respectively. The ratio $d_{Er}/d_{\text{optical}} = 2.1$ agrees with the conclusion in [52, 79, 80] that the electrodynamic diameter is about twice the optical diameter.

Appendix B. Ion motion

Ion motion can be an important mechanism for slow positive streamers [31, 32], especially when the streamer velocity becomes comparable to the ion drift velocity. However, as

Table C1. Additional positive ion conversion and electron–ion recombination reactions. T (K) and T_e (K) are gas and electron temperatures, respectively. T_e is computed as $T_e = 2\epsilon_e/3k_B$ with the mean electron energy ϵ_e obtained from BOLSIG+ [59].
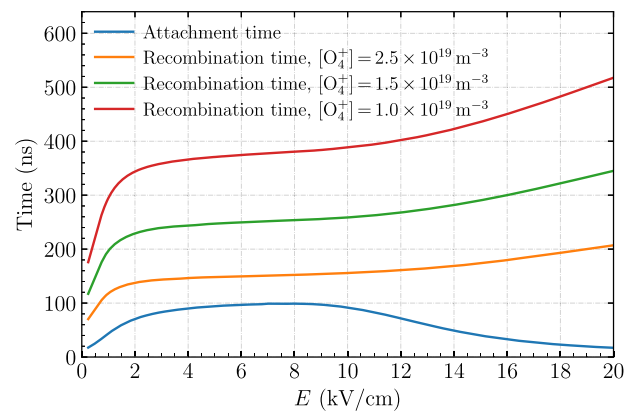
No.	Reaction	Reaction rate coefficient	Reference
Positive ion conversion			
R14	$N_2^+ + O_2 \rightarrow O_2^+ + N_2$	$k_{14} = 6.0 \times 10^{-17}(\frac{300}{T})^{0.5}$ m^3 s^{-1}	[53]
R15	$N_2^+ + N_2 + M \rightarrow N_4^+ + M$	$k_{15} = 5.0 \times 10^{-41}(\frac{300}{T})^{2.2}$ m^6 s^{-1}	[53]
R16	$N_4^+ + O_2 \rightarrow O_2^+ + N_2 + N_2$	$k_{16} = 2.5 \times 10^{-16}$ m^3 s^{-1}	[53]
R17	$O_2^+ + O_2 + M \rightarrow O_4^+ + M$	$k_{17} = 2.4 \times 10^{-42}(\frac{300}{T})^{3.2}$ m^6 s^{-1}	[53]
Electron–ion recombination			
R18	$e + N_2^+ + M \rightarrow N_2 + M$	$k_{18} = 6.0 \times 10^{-39}(\frac{300}{T_e})^{1.5}$ m^6 s^{-1}	[53]
R19	$e + O_2^+ + M \rightarrow O_2 + M$	$k_{19} = 6.0 \times 10^{-39}(\frac{300}{T_e})^{1.5}$ m^6 s^{-1}	[53]
R20	$e + N_2^+ \rightarrow N_2$	$k_{20} = 1.5 \times 10^{-13}$ m^3 s^{-1}	[81]
R21	$e + O_2^+ \rightarrow O_2$	$k_{21} = 1.5 \times 10^{-13}$ m^3 s^{-1}	[81]
R22	$e + N_4^+ \rightarrow N_2 + N_2$	$k_{22} = 2.0 \times 10^{-12}(\frac{300}{T_e})^{0.5}$ m^3 s^{-1}	[53]
R23	$e + O_4^+ \rightarrow O_2 + O_2$	$k_{23} = 1.4 \times 10^{-12}(\frac{300}{T_e})^{0.5}$ m^3 s^{-1}	[53]
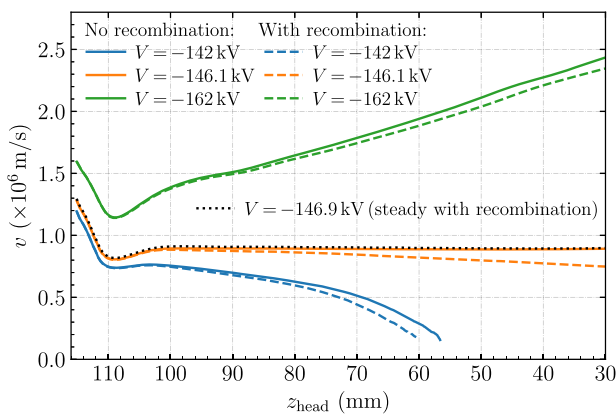
Figure C1. Comparison of negative streamer propagation with and without the additional reactions given in table C1. The streamer velocity v is shown versus the streamer position z_{head} for three different streamers corresponding to figure 2. With electron–ion recombination, a steady negative streamer is found at $V = -146.9$ kV.

Figure C2. The electron attachment time and $e + O_4^+$ recombination time versus the electric field E. The $e + O_4^+$ recombination time depends on the O_4^+ density, which in our simulations was generally below 10^{19} m^{-3}.

was discussed in section 4.3, a negative streamer needs to propagate with at least the maximal electron drift velocity, which is approximately two orders of magnitude larger than the ion drift velocity. As a result, ion motion has little effect on the propagation of the negative streamers simulated in this paper. Note that in regions where the ion density is much higher than the electron density ions contribute significantly to the plasma conductivity, but this conductivity is then much lower than it is near the streamer head.

Appendix C. Effect of electron–ion recombination reactions

We here investigate the effect of including the additional positive ion conversion and electron–ion recombination reactions given in table C1. Figure C1 shows how accelerating, steady and negative streamers are affected by including these reactions. The simulations were performed in domain A, see section 3.1. With the extra reactions, negative streamers are slightly slower due to increased conductivity loss behind the streamer head. However, the effect is rather small, and the steady applied voltage changes by only 0.5%.

O_4^+ is typically the dominant positive ion in streamer discharges at atmospheric pressure air. In figure C2, the electron attachment time is compared with the $e + O_4^+$ recombination time, where these time scales are given by the inverse of the respective reaction frequencies. The $e + O_4^+$ recombination time depends on the O_4^+ density, and in our simulations, O_4^+ densities were generally below 10^{19} m^{-3}. Including positive ion conversion and electron–ion recombination—which we in hindsight maybe should have done—would therefore not significantly alter the results presented in this paper.

In contrast, for positive streamers in air, the $e + O_4^+$ recombination time can be shorter than the electron attachment time due to a low internal electric field and high O_4^+ density, so that electron–ion recombination plays a significant role [31, 32, 34, 36, 57].

ORCID iDs

Baohong Guo ⬥ https://orcid.org/0000-0001-8368-5014
Xiaoran Li ⬥ https://orcid.org/0000-0003-3354-9078
Ute Ebert ⬥ https://orcid.org/0000-0003-3891-6869
Jannis Teunissen ⬥ https://orcid.org/0000-0003-0811-5091

References

[1] Nijdam S, Teunissen J and Ebert U 2020 *Plasma Sources Sci. Technol.* **29** 103001
[2] Huiskamp T 2020 *Plasma Sources Sci. Technol.* **29** 023002
[3] Gallimberti I 1979 *J. Phys. Colloq.* **40** C7-193–C7-250
[4] Lalande P, Bondiou-Clergerie A, Bacchiega G and Gallimberti I 2002 *C. R. Phys.* **3** 1375–92
[5] Pasko V P 2007 *Plasma Sources Sci. Technol.* **16** S13–29
[6] Ebert U, Nijdam S, Li C, Luque A, Briels T and van Veldhuizen E 2010 *J. Geophys. Res.: Space Phys.* **115** A00E43
[7] Kim H-H 2004 *Plasma Process. Polym.* **1** 91–110
[8] Keidar M, Shashurin A, Volotskova O, Ann Stepp M, Srinivasan P, Sandler A and Trink B 2013 *Phys. Plasmas* **20** 057101
[9] Starikovskaia S M 2014 *J. Phys. D: Appl. Phys.* **47** 353001
[10] Raizer Yuri P 1991 *Gas Discharge Physics* (Berlin: Springer)
[11] van Veldhuizen E M 2000 *Electrical Discharges for Environmental Purposes: Fundamentals and Applications* (Huntington: Nova Science)
[12] Seeger M, Votteler T, Ekeberg J, Pancheshnyi S and Sánchez L 2018 *IEEE Trans. Dielectr. Electr. Insul.* **25** 2147–56
[13] Briels T M P, Kos J, Winands G J J, van Veldhuizen E M and Ebert U 2008 *J. Phys. D: Appl. Phys.* **41** 234004
[14] Starikovskiy A Y and Aleksandrov N L 2020 *Plasma Sources Sci. Technol.* **29** 075004
[15] Reess T, Ortega P, Gibert A, Domens P and Pignolet P 1995 *J. Phys. D: Appl. Phys.* **28** 2306–13
[16] Taylor M J *et al* 2008 *Geophys. Res. Lett.* **35** L14812
[17] Arevalo L and Cooray V 2011 *J. Phys. D: Appl. Phys.* **44** 315204
[18] Kochkin P O, van Deursen A P J and Ebert. U 2014 *J. Phys. D: Appl. Phys.* **47** 145203
[19] Malagón-Romero A and Luque A 2019 *Geophys. Res. Lett.* **46** 4029–38
[20] Tilles J N, Liu N, Stanley M A, Krehbiel P R, Rison W, Stock M G, Dwyer J R, Brown R and Wilson J 2019 *Nat. Commun.* **10** 1648
[21] Jacob K, Shi F, Liu N, Dwyer J and Tilles J 2020 *Geophys. Res. Lett.* **47** e2020GL088244
[22] Scholten O *et al* 2021 *Sci. Rep.* **11** 16256
[23] Yi W J and Williams P F 2002 *J. Phys. D: Appl. Phys.* **35** 205–18
[24] Wang D, Jikuya M, Yoshida S, Namihira T, Katsuki S and Akiyama H 2007 *IEEE Trans. Plasma Sci.* **35** 1098–103
[25] Huiskamp T, Sengers W, Beckers F J C M, Nijdam S, Ebert U, van Heesch E J M and Pemen A J M 2017 *Plasma Sources Sci. Technol.* **26** 075009
[26] Babaeva N Y and Naidis G V 1997 *IEEE Trans. Plasma Sci.* **25** 375–9
[27] Liu N 2004 *J. Geophys. Res.* **109** A04301
[28] Luque A, Ratushnaya V and Ebert U 2008 *J. Phys. D: Appl. Phys.* **41** 234005
[29] Naidis G V 2009 *Phys. Rev.* E **79** 057401
[30] Babaeva N Y and Naidis G V 2016 *Phys. Plasmas* **23** 083527
[31] Niknezhad M, Chanrion O, Holbøll J and Neubert T 2021 *Plasma Sources Sci. Technol.* **30** 115014
[32] Li X, Guo B, Sun A, Ebert U and Teunissen J 2022 *Plasma Sources Sci. Technol.* **31** 065011
[33] Winands G J J, Liu Z, Pemen A J M, van Heesch E J M and Yan K 2008 *J. Phys. D: Appl. Phys.* **41** 234001
[34] Starikovskiy A Y, Aleksandrov N L and Shneider M N 2021 *J. Appl. Phys.* **129** 063301
[35] Pancheshnyi S V and Starikovskii A Y 2004 *Plasma Sources Sci. Technol.* **13** B1–5
[36] Francisco H, Teunissen J, Bagheri B and Ebert U 2021 *Plasma Sources Sci. Technol.* **30** 115007
[37] Phelps C T 1971 *J. Geophys. Res.* **76** 5799–806
[38] Allen N L and Ghaffar A 1995 *J. Phys. D: Appl. Phys.* **28** 331–7
[39] Qin J and Pasko V P 2014 *J. Phys. D: Appl. Phys.* **47** 435202
[40] Phelps C T and Griffiths R F 1976 *J. Appl. Phys.* **47** 2929–34
[41] Griffiths R F and Phelps C T 1976 *Q. J. R. Meteorol. Soc.* **102** 419–26
[42] Allen N L and Boutlendj M 1991 *IEE Proc. A Sci. Meas. Technol. UK* **138** 37
[43] Niemeyer L 1995 *IEEE Trans. Dielectr. Electr. Insul.* **2** 510–28
[44] Allen N L and Mikropoulos P N 1999 *J. Phys. D: Appl. Phys.* **32** 913–9
[45] Teunissen J and Ebert U 2017 *J. Phys. D: Appl. Phys.* **50** 474001
[46] Teunissen J and Ebert U 2018 Afivo: a framework for quadtree/octree AMR with shared-memory parallelization and geometric multigrid methods *Comput. Phys. Commun.* **233** 156–66
[47] Bagheri B *et al* 2018 *Plasma Sources Sci. Technol.* **27** 095002
[48] Li X, Dijcks S, Nijdam S, Sun A, Ebert U and Teunissen J 2021 *Plasma Sources Sci. Technol.* **30** 095002
[49] Wang Z, Sun A and Teunissen J 2022 *Plasma Sources Sci. Technol.* **31** 015012
[50] Phelps A V and Pitchford L C 1985 *Phys. Rev.* A **31** 2932–49
[51] Pancheshnyi S 2013 *J. Phys. D: Appl. Phys.* **46** 155201
[52] Pancheshnyi S, Nudnova M and Starikovskii A 2005 *Phys. Rev.* E **71** 016407
[53] Kossyi I A, Kostinsky A Y, Matveyev A A and Silakov V P 1992 *Plasma Sources Sci. Technol.* **1** 207–20
[54] Luque A, Ebert U, Montijn C and Hundsdorfer W 2007 *Appl. Phys. Lett.* **90** 081501
[55] Zheleznyak M B, Mnatsakanyan A K and Sizykh S V 1982 *High Temp.* **20** 357–62
[56] Bagheri B and Teunissen J 2019 *Plasma Sources Sci. Technol.* **28** 045013
[57] Francisco H, Bagheri B and Ebert U 2021 *Plasma Sources Sci. Technol.* **30** 025006
[58] Bourdon A, Pasko V P, Liu N Y, Célestin S, Ségur P and Marode E 2007 *Plasma Sources Sci. Technol.* **16** 656–78
[59] Hagelaar G J M and Pitchford L C 2005 *Plasma Sources Sci. Technol.* **14** 722–33
[60] Phelps database (N_2, O_2) www.lxcat.net (retrieved 1 December 2020)
[61] Zhang Q-Z, Nguyen-Smith R T, Beckfeld F, Liu Y, Mussenbrock T, Awakowicz P and Schulze J 2021 *Plasma Sources Sci. Technol.* **30** 075017
[62] Teunissen J and Schiavello F 2022 Geometric multigrid method for solving Poisson's equation on octree grids with irregular boundaries (arXiv:2205.09411 [physics])
[63] Pancheshnyi S V, Sobakin S V, Starikovskaya S M and Starikovskii A Y 2000 *Plasma Phys. Rep.* **26** 1054–65
[64] Hansen E W and Law P-L 1985 *J. Opt. Soc. Am.* A **2** 510–20
[65] Babaeva N Y and Naidis G V 1996 *J. Phys. D: Appl. Phys.* **29** 2423–31
[66] van Veldhuizen E M and Rutgers W R 2002 *J. Phys. D: Appl. Phys.* **35** 2169–79
[67] Celestin S and Pasko V P 2011 *J. Geophys. Res.: Space Phys.* **116** A03315
[68] Gallimberti I and Wiegart N 1986 *J. Phys. D: Appl. Phys.* **19** 2351–61
[69] Bujotzek M, Seeger M, Schmidt F, Koch M and Franck C 2015 *J. Phys. D: Appl. Phys.* **48** 245201

[70] Seeger M, Avaheden J, Pancheshnyi S and Votteler T 2017 *J. Phys. D: Appl. Phys.* **50** 015207

[71] Morrow R and Lowke J J 1997 *J. Phys. D: Appl. Phys.* **30** 614–27

[72] Luque A and Ebert U 2014 *New J. Phys.* **16** 013039

[73] Briels T M P, Kos J, van Veldhuizen E M and Ebert U 2006 *J. Phys. D: Appl. Phys.* **39** 5201–10

[74] Briels T M P, van Veldhuizen E M and Ebert U 2008 *J. Phys. D: Appl. Phys.* **41** 234008

[75] Nijdam S, van de Wetering F M J H, Blanc R, van Veldhuizen E M and Ebert U 2010 *J. Phys. D: Appl. Phys.* **43** 145204

[76] Ebert U, van Saarloos W and Caroli C 1997 *Phys. Rev.* E **55** 1530–49

[77] Ebert U, van Saarloos W and Caroli C 1996 *Phys. Rev. Lett.* **77** 4178–81

[78] Bagheri B, Teunissen J and Ebert U 2020 *Plasma Sources Sci. Technol.* **29** 125021

[79] Nudnova M M and Starikovskii A Y 2008 *J. Phys. D: Appl. Phys.* **41** 234003

[80] Luque A and Ebert U 2009 *Nat. Geosci.* **2** 757–60

[81] Tochikubo F and Arai H 2002 *Japan. J. Appl. Phys.* **41** 844–52